DOT/FAA/AR-99/8,V

Office of Aviation Research
Washington, D.C. 20591

Improved Barriers to Turbine Engine Fragments: Final Annual Report

June 2002

Final Report

U.S. Department of Transportation
Federal Aviation Administration

NOTICE

This report is available at the Federal Aviation Administration William J. Hughes Technical Center's Full-Text Technical Reports page: actlibrary.tc.faa.gov in Adobe Acrobat portable document format (PDF).

Technical Report Documentation Page

1. Report No.	2. Government Accession No.	3. Recipient's Catalog No.
DOT/FAA/AR-99/8-V		

4. Title and Subtitle	5. Report Date
IMPROVED BARRIERS TO TURBINE ENGINE FRAGMENTS: FINAL ANNUAL REPORT	June 2002
	6. Performing Organization Code

7. Author(s)	8. Performing Organization Report No.
Donald A. Shockey, David C. Erlich, and Jeffrey W. Simons	

9. Performing Organization Name and Address	10. Work Unit No. (TRAIS)
SRI International 333 Ravenswood Avenue Menlo Park, CA 94025-3493	11. Contract or Grant No. 95-G-010

12. Sponsoring Agency Name and Address	13. Type of Report and Period Covered
U.S. Department of Transportation Federal Aviation Administration Office of Aviation Research Washington, DC 20591	Final Report
	14. Sponsoring Agency Code ANE-100, ANM-100

15. Supplementary Notes

The FAA William J. Hughes Technical Center COTR: William Emmerling and Donald Altobelli.

16. Abstract

This final annual technical report describes the progress made during year 4 of the SRI International Phase II effort to develop a computational capability for designing lightweight fragment barriers for commercial aircraft. Fabrics of high-strength polymers have proven to be excellent candidates for these barriers.

Previous large-scale fragment impact testing of corner peg-mounted fabric barriers indicated that the failure of the fabric around the pegged hole was a significant factor in the barrier's effectiveness. Thus, SRI designed and implemented a laboratory test to characterize fabric failure behavior in the vicinity of a pegged hole. A series of these fabric corner failure tests in both Zylon and Kevlar fabrics determined that significant energy can be absorbed in corner tearing. These tests also showed the effects of various parameters on this energy.

SRI then performed a second series of large-scale fragment impact tests at its remote test site, using stand-alone fabric barriers attached to a rigid frame through pegs near the four corners. The pegged corner holes were positioned far enough from the fabric edges to allow significant corner tearing without complete corner detachment. Tests revealed a relatively small effect of fragment roll angle and a large effect of impact location (with respect to the center of the barrier) upon the ballistic efficiency of the barrier. In some cases, Kevlar could be as effective as (or more effective than) Zylon, due to the larger fraction of impact energy consumed in producing corner tearing. A considerable database of large-scale fragment impact tests into Zylon and Kevlar fabric ballistic barriers is now available for fabric computational model refinement and verification.

A simplified finite element fabric model has been developed for use as a design tool for choosing or evaluating parameters for fragment barriers. The design tool uses a continuum description of the fabric, and the calculations run quickly (about 10 min for a 3000-element simulation of a gas-gun test using 6 processors on a Linux cluster) and easily, allowing evaluation of changes in size of fabric, number of layers, and method of gripping.

The reliability of the model was evaluated by performing computational simulations of push tests, laboratory gas gun impact tests, and large-scale impact tests of Zylon fabric. The computed deformation and failure behavior and the energy absorbed by the fabric during penetration agreed with measurements to within about 20% for most cases. This report also discusses limitations of the model in its current state.

17. Key Words	18. Distribution Statement
Aircraft engine fragments, Fragment barriers, PBO armor, Zylon	This document is available to the public through the National Technical Information Service (NTIS), Springfield, Virginia 22161.

19. Security Classif. (of this report)	20. Security Classif. (of this page)	21. No. of Pages	22. Price
Unclassified	Unclassified	50	

ACKNOWLEDGMENTS

The authors are grateful for the contributions of their colleagues and collaborators during the course of this work. Mr. Tadao Kuroki of Toyobo, Inc., provided the Zylon material. Mr. William Emmerling and Mr. Donald Altobelli of the FAA Technical Center provided continual guidance. We greatly appreciate the interest and encouragement of Mr. Timoleon Mouzakis and Mr. Michael Dostert of the FAA Regional Offices.

TABLE OF CONTENTS

LIST OF FIGURES

LIST OF TABLES

EXECUTIVE SUMMARY

This final annual technical report describes the progress made during year 4 (January 1 through September 30, 2001) of the SRI International (hereafter referred to as SRI) Phase II effort to develop a computational capability for designing lightweight fragment barriers for commercial aircraft. Fabrics of high-strength polymers have been shown to be excellent candidates for these barriers.

Previous large-scale fragment impact testing of corner peg-mounted fabric barriers (performed at SRI's remote test site) showed that failure of the fabric around the pegged hole was a significant factor in the barrier's effectiveness. SRI designed and implemented a laboratory test to characterize fabric failure behavior in the vicinity of a pegged hole. A series of these fabric corner failure tests in both Zylon and Kevlar fabrics determined that significant energy can be absorbed in corner tearing and showed the effect of various parameters on this energy.

SRI then performed a second series of large-scale fragment impact tests at Corral Hollow Experimental Site (CHES), SRI's remote test site near Tracy, California, in which fabric barriers were attached to a rigid fuselage frame through pegs near the four corners. The pegged corner holes were positioned far enough from the fabric edges to allow significant corner tearing without complete corner detachment. Tests revealed a relatively small effect of fragment roll angle and a large effect of impact location (with respect to the center of the barrier) on the ballistic efficiency of the barrier. In some cases, Kevlar could be as effective as (or more effective than) Zylon, due to the larger fraction of impact energy consumed in producing corner tearing. A considerable amount of data of large-scale fragment impact tests into Zylon and Kevlar fabric ballistic barriers is now available for refining and verifying computational models.

SRI has developed a simplified finite element fabric model for use as a design tool for choosing or evaluating parameters for fragment barriers. The design tool uses a continuum description of the fabric, and the calculations run quickly (about 10 min for a 3000-element simulation of a gas gun test using 6 processors on a Linux cluster) and easily, allowing evaluation of changes in size of fabric, number of layers, and method of gripping.

SRI evaluated the reliability of the model by performing computational simulations of push tests, laboratory gas gun impact tests, and large-scale impact tests of Zylon fabric. The computed deformation and failure behavior and the energy absorbed by the fabric during penetration agreed with measurements to within about 20% for most cases.

In this report, the first section reviews the motivation for this program and briefly summarizes progress previously achieved. The second section describes laboratory tests to characterize the failure of fabric barriers around corner pegs and a second series of large-scale impact tests on the fabric barriers performed at SRI's remote test site. The third section describes progress on development of the computational model. The fourth section lists publications, presentations, and briefly describes two Federal Aviation Administration Airworthiness Assurance Center of Excellence Grants awarded in late government fiscal year (FY) 2001 to transfer the technology to the commercial aircraft community.

INTRODUCTION AND BACKGROUND

Over the years, several civil aircraft accidents with catastrophic consequences have occurred when fragments from in-flight engine failures damaged critical aircraft components. To reduce the probability of catastrophic consequences from engine failures, the Federal Aviation Administration (FAA) established the Aircraft Catastrophic Failure Prevention Program (ACFPP) [1] to develop and apply advanced technologies and methods for assessing, preventing, or mitigating the effects of such failures. In support of the ACFPP objective, SRI International (hereafter referred to as SRI) is conducting research aimed at developing lightweight barrier systems for turbine engine fragments.

In Phase I of this program, SRI reviewed the rich body of armor technology held by the Department of Defense to identify concepts, materials, and armor designs that could lead to practical barriers to engine fragments on commercial aircraft [2]. Highly ordered, highly crystalline, high-molecular-weight polymers were identified as the advanced materials holding greatest promise for engine fragment barriers on aircraft. Specifically, fabrics of certain aramids (Kevlar and Twaron), polyethylenes (Spectra and Dyneema), and polybenzobisoxazole (PBO Zylon) appeared able to provide a useful measure of ballistic protection in the most weight-efficient manner. Furthermore, some of these materials appear to have sufficient flame resistance, water absorption resistance, and thermal and acoustic insulation properties to serve as building blocks for barriers.

In Phase II, SRI conducted a combined experimental and modeling research program to characterize the ballistic properties of these high-strength fabrics and develop a computational capability for designing the barriers. During the first 3 years of the Phase II program [3, 4, and 5], small- and large-scale impact tests performed at SRI and full-scale fuselage impact experiments performed at Naval Air Warfare Center (NAWC) China Lake, using real fragments or fragment-simulating projectiles, confirmed that lightweight barriers made of a few plies of these fabrics absorb substantial fragment energy. These tests indicated how the ballistic effectiveness of the fabric varied in response to changes in the number of fabric plies, boundary conditions (how the fabric was gripped), and fragment sharpness.

To assist in model development, tensile and friction properties of the fabric yarns were measured at several strain rates. In addition, quasi-static penetration tests were performed with a tensile machine and monitored with an audio-video camera to elucidate the phenomenology and evolution of fabric failure. Three different fabric failure mechanisms were observed and the effects of multiple fabric plies and gripping geometry were investigated.

Computational models were developed at two levels of material detail to facilitate the design of barrier structures and assist in their evaluation. The more detailed model treats individual yarns of the fabric explicitly, accounting for yarn geometry, properties, interactions with each other, and failure mechanisms. This model, implemented with brick elements in the LS-DYNA3D finite element code, was used to examine postulated ballistic scenarios and compute the failure behavior of yarns and fabrics under impact scenarios. Fragment barriers were designed using the

insights gained from the simulations, the barriers were then constructed, and their performance was evaluated in full-scale fragment impact experiments on a fuselage.

In the less detailed "engineering design" model, the fabric is modeled in shell-element form, which decreases the computation time significantly. This model was used to simulate fragment impact tests and is intended for use by aeronautical engineers in designing fragment barriers.

BALLISTIC TESTING OF FABRIC BARRIERS

The series of large-scale impact tests performed from September to November 2000, using the 6-in.-bore gas gun located at The Corral Hollow Experimental Site (CHES), SRI's remote test site near Tracy, California, examined the effectiveness of the fabric barriers to realistic fragment impact scenarios.

As discussed in the previous technical report [5], the results showed the importance of barrier-airframe attachment conditions; that tearing of the fabric around each corner peg could be used as an energy-absorbing mechanism. Therefore, before conducting further ballistic testing, SRI performed a series of quasi-static laboratory fabric corner failure tests to gain an understanding of the phenomenology of fabric corner failure and determine the energy absorbed in fabric failure around a peg.

FABRIC CORNER FAILURE TESTS.

A laboratory test, called the fabric corner failure test, was designed to examine fabric behavior in the vicinity of a pegged corner. As shown in figure 1, the test is performed on the MTS servo-hydraulic mechanical testing machine and uses some of the same fixtures from the previously reported [3] quasi-static penetration (pull) tests and yarn pullout tests. A square sheet of fabric is folded in half and tightly gripped along one diagonal to form two triangular test specimens. A square hole is cut in the corner of each specimen at a specific distance from the corner. The fabric is inserted between two transparent acrylic plates attached to a clevis, a cylindrical peg is inserted through the hole in the fabric and the plates, and the specimen is pulled at a constant rate, usually until the peg tears through to the fabric edge. The stroke (deflection of the grip with respect to the peg) and the load (force that the fabric exerts on the peg) are continuously recorded, while a video camera and microphone capture detailed visual images and acoustic emissions of the fabric deformation and failure around the pegged hole.

TEST MATRIX. A matrix for the corner pull tests is given in table 1, including test parameters, resultant energy absorbed, E_A, and the quantitative yarn damage results. Parameters that were varied included:

- Fabric Material — The baseline material was Zylon 35x35; a few tests were performed on Zylon 35x35, Zylon 40x40, and Kevlar 32x32. The Zylon fabrics had 500-denier yarns, while the Kevlar fabric had 400-denier yarns. A more complete description of the fabrics may be found in table 4 of reference 3.

- Pull rate — The baseline pull rate was 7.5 in./s (19 cm/s), which is the fastest rate available on the MTS machine; a few tests were performed at 0.075 in./s (0.19 cm/s).

- Hole size (equals peg diameter), P (in figure 1 and table 1) — The baseline size was 0.75 in. (1.9 cm); a few tests were performed with size of 0.25 in. (0.6 cm).

- Distance of hole (peg) from fabric edges, D_e — from 1.0 to 5.0 in. (2.5 to 12.7 cm).

- Distance of hole (peg) from grip, D_g — from 4.0 to 8.2 in. (10.2 to 20.8 cm).

- Shape of the fabric test piece — The baseline geometry was a right isosceles triangle (half of a square sheet folded along a diagonal) tightly gripped for 5 in. (12.7 cm) along the midpoint of the hypotenuse, with a 0.5-in.- (1.3-cm)-wide gap on each side to clear the end of the clamping bar. Other configurations decreased the length of the gripped section, increased the gap at the end of the grip, or eliminated the material outside the lines perpendicular to the grip at each end (see figure 1).

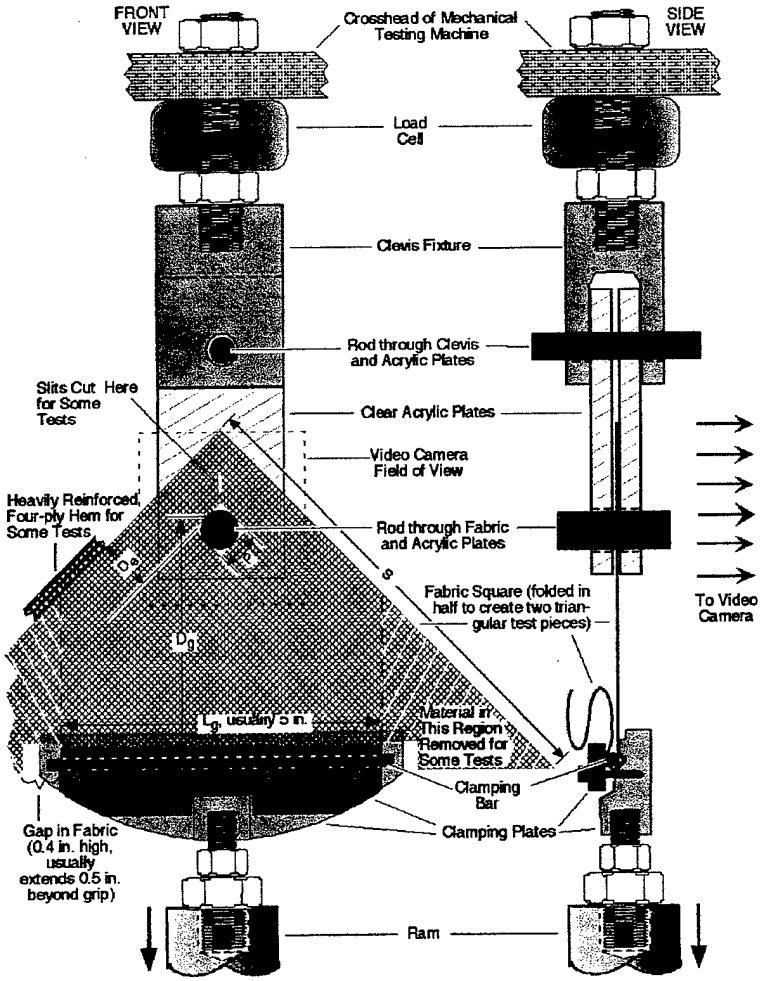

FIGURE 1. EXPERIMENTAL DESIGN FOR FABRIC CORNER FAILURE TESTS

TABLE 1. CORNER PULL TEST MATRIX

Test No.[a]	Material and Mesh		Dimensions (in.)—See Fig. 1 Fabric Size (S)	Peg (P) (or Hole)	Distance to: Edge (D_e)	Grip (D_g)	Pull Rate (in./s)	Energy Absorbed (E_A) (ft-lb)	(J)	No. of Yarns Broken	Pulled Out	Comments Note: Baseline geometry[b] unless stated otherwise.
3A	Zylon	35x35	12	0.75	3.0	4.0	7.5	N.A.	N.A.	95	5	
3B	Zylon	35x35	12	0.75	3.0	4.0	0.075	N.A.	N.A.	155	0	
4A	Zylon	35x35	12	0.75	1.0	6.8	7.5	20	28	0	35	
4B	Zylon	35x35	12	0.75	2.0	5.4	7.5	65	88	69	21	
5A	Zylon	35x35	10	0.75	2.0	4.0	7.5	65	87	51	21	
5B	Zylon	35x35	12	0.75	1.5	6.1	7.5	53	72	34	23	
6A	Zylon	35x35	9	0.75	1.5	4.0	7.5	46	62	31	21	
7A	Zylon	35x35	12	0.75	3.0	4.0	7.5	132	179	141	12	
7B	Zylon	35x35	16	0.75	2.0	8.2	7.5	66	89	59	17	
8A	Zylon	35x35	16	0.75	5.0	4.0	7.5	218	296	300	8	
8B	Zylon	35x35	12	0.75	2.0	5.4	7.5	57	78	56	16	Repeat of Test 4B
9A	Zylon	35x35	9.75	0.25	2.0	4.0	7.5	49	67	65	13	
9B	Zylon	35x35	9.75	0.25	2.0	4.0	0.075	59	80	47	23	
10A	Zylon	35x35	10	0.75	2.0	4.0	7.5	71	96	60	22	2.5-in.-long grip, 1.75-in.-long gaps beyond
10B	Zylon	35x35	10	0.75	2.0	4.0	7.5	65	88	65	24	2.5-in.-long grip, gaps extend to fabric edge
11A	Zylon	35x35	10	0.75	2.0	4.0	7.5	62	84	58	9	Fabric removed beyond grip's ends (see Fig. 1)
12A	Zylon	35x35	10	0.75	2.0	4.0	7.5	67	90	62	22	5-in.-long grip, gaps extending to fabric edge
13A	Zylon	35x35	12	0.75	3.0	4.0	7.5	105	142	128	33	Fabric removed beyond grip's ends (see Fig. 1)
14A	Zylon	40x40	12	0.75	3.0	4.0	7.5	155	210	203	0	
15A	Zylon	30x30	12	0.75	3.0	4.0	7.5	145	197	136	0	
15B	Zylon	30x30	12	0.75	3.0	4.0	0.075	233	315	108	0	
Tests 16-18 (A & B), 19B have slits between the hole and fabric corner.											Slit parameters ->	No. / Direction[c] / Length / Gap / Starting at[d]
16A	Zylon	35x35	12	0.75	3.0	4.0	7.5	107	145	N.A.	N.A.	5 / Diagonal / 0.35 / 0.35 / 0.0
16B	Zylon	35x35	12	0.75	3.0	4.0	7.5	97	131	N.A.	N.A.	5 / Diagonal / 0.35 / 0.35 / 0.35
17A	Zylon	35x35	12	0.75	3.0	4.0	7.5	126	170	N.A.	N.A.	1 / Diagonal / 0.35 / —— / 0.35
17B	Zylon	35x35	12	0.75	3.0	4.0	7.5	125	170	N.A.	N.A.	2 / Diagonal / 0.35 / 1.4 / 0.35
18A	Zylon	35x35	12	0.75	3.0	4.0	7.5	80	109	N.A.	N.A.	4 / Vert./Hor. / 0.25 / 0.5 / 0.25
18B	Zylon	35x35	12	0.75	3.0	4.0	7.5	113	153	N.A.	N.A.	2 / Vert./Hor. / 0.25 / 1.0 / 0.25
Tests 19 A and B have a 4-ply, 0.5-in.-wide hem around the fabric's edge.												
19A	Zylon	35x35	10[e]	0.75	2.0[e]	4.0	7.5	143	194	194[e]	7[e]	
19B	Zylon	35x35	10[e]	0.75	2.0[e]	4.0	7.5	206	279	N.A.	N.A.	3 / Diagonal / 0.35 / 0.35 / 0.35
20A	Kevlar	32x32	12	0.75	3.0	4.0	7.5	78	105	135	0	
20B	Kevlar	32x32	12	0.75	3.0	4.0	0.075	90	122	135	20	

[a] Tests A and B use two triangles from the same specimen.

[b] Baseline geometry: square specimen, gripped for 5 in. along diagonal (L_g in Fig. 1), 0.5-in.-long gaps in fabric beyond gripped ends (no hem or slits).

[c] Slits are cut either along the diagonal or alternating between vertical and horizontal directions. Slit dimensions are in inches, measured in the slit direction.

[d] Distance of the corner of the pegged hole nearest the fabric corner to the start of the first slit.

[e] S is distance between opposite hems; D_e is distance of hem to closest edge of pegged hole; broken and pulled-out yarns include those from hem.

Some tests were performed with modifications to the fabric test piece to increase (e.g., a hem around the fabric, as in tests 19A, and B) or decrease (e.g., slits cut in the fabric between the hole and the corner, as in tests 16-18A, B and 19B) the energy needed to tear through the fabric.

TEST RESULTS. Figure 2 shows a typical load-stroke curve (from test 8A). First, the fabric deformed around the peg without any yarn rupture as the load rose to an initial peak. Yarn rupture began at the peak and the load dropped to a rough plateau as yarn rupture continued intermittently.* As the peg neared the fabric edge and the force necessary to overcome the frictional forces between yarns became less than that needed to rupture the yarn, the failure mode switched from local rupture to yarn pullout, and the load decreased to zero as the remaining yarns were pulled out of the fabric. The test results were repeatable within ±10% for both energy absorbed and yarn failure.

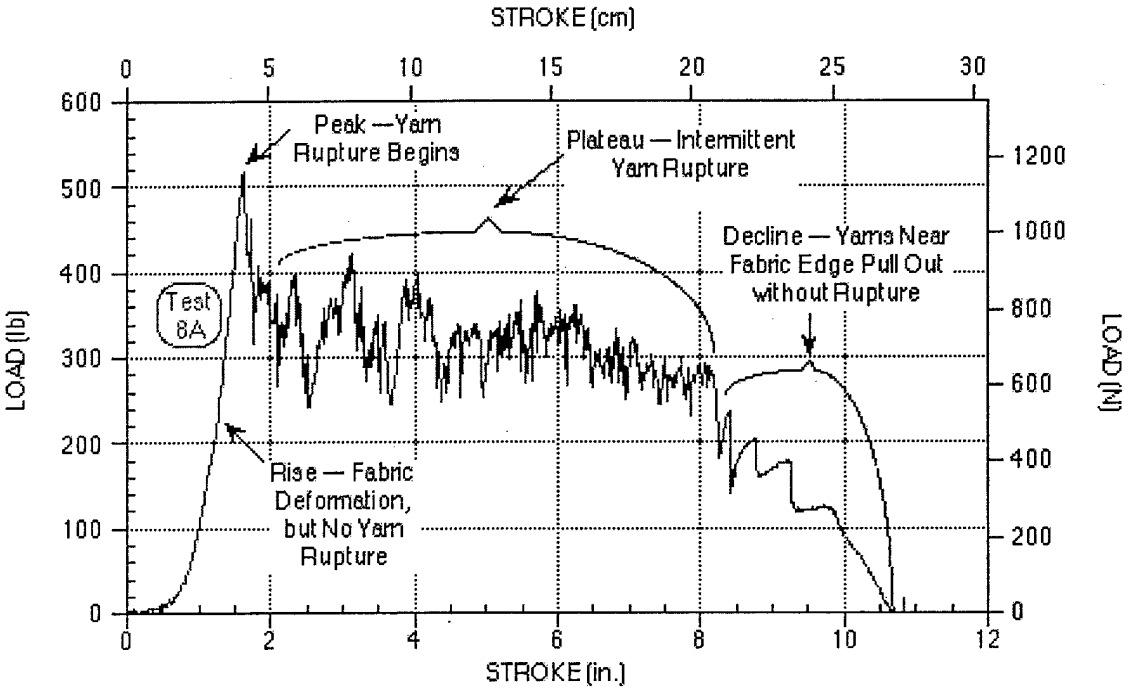

FIGURE 2. TYPICAL LOAD-STROKE CURVE FROM CORNER PULL TEST

In test 8A, for example, the distance between the hole and the fabric edges, D_e, was 5 in. The plateau of intermittent yarn rupture extended over more than 6 in. of stroke; 300 yarns ruptured (167 in one direction and 133 in the other) before the final eight yarns were pulled out (see figure 3). On the other hand, in test 4A, where D_e was only 1 in., no yarns were ruptured; all 35 yarns between the hole and fabric edge failed by yarn pullout (see figure 4).

* There are local peaks within the plateau that reached levels close to the initial peak. These later peaks may identify where the rupture switches from yarns in one direction to yarns in the other perpendicular direction.

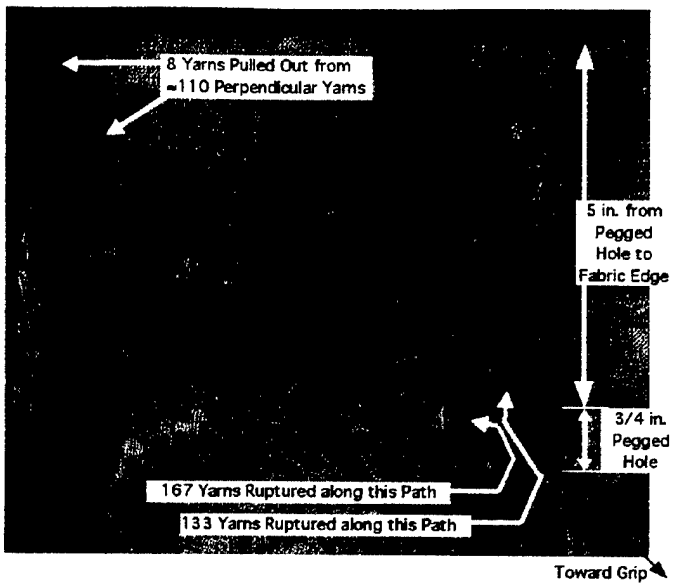

FIGURE 3. PHENOMENOLOGY OF FABRIC FAILURE IN CORNER PULL TEST 8A

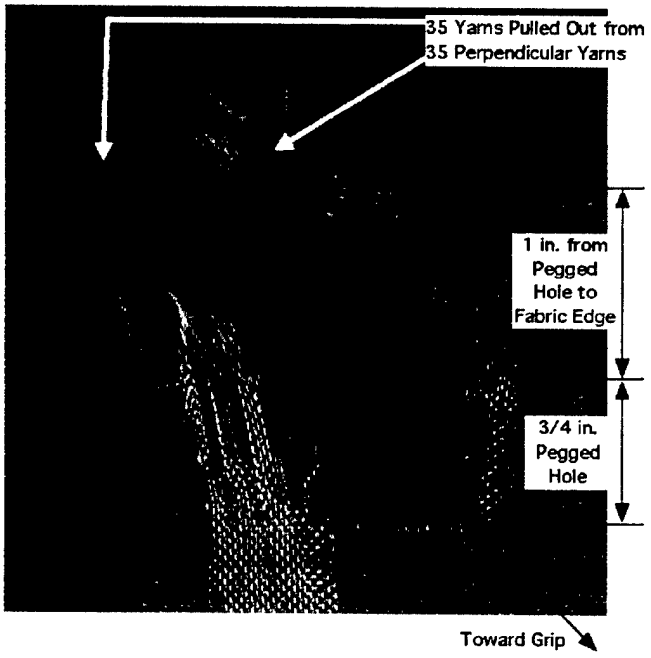

FIGURE 4. PHENOMENOLOGY OF FABRIC FAILURE IN CORNER PULL TEST 4A

The effect of D_e on energy absorption can be seen clearly in the next two figures. Four tests were performed with the baseline material (Zylon 35x35), pull rate (7.5 in./s), hole size (P = 0.75 in.), and specimen geometry (with D_g = 4 in.), while D_e measured 1.5 in. (test 6A), 2 in. (5A), 3 in. (7A), and 5 in. (test 8A), respectively. The load-stroke curves are shown in figure 5, along with the curve for test 20A, which used the Kevlar fabric and a D_e of 3 in. For Zylon, the curves all have similar peaks, roughly 500 lb (2200 N) at a stroke of around 1.6 in. (4 cm), then dropped off to plateaus with a height of about 310 lb (1380 N). The farther the peg is from the fabric edge to

begin with, the longer the plateau section. For Kevlar, the loads peak at around 350 lb (1560 N), plateau at around 175 lb (780 N), and the plateau length is the same as that for the Zylon test with the identical D_e. The absorbed energy, E_A, as a function of D_e is shown in figure 6.

Note: It should be noted that test 20A was terminated before complete failure.

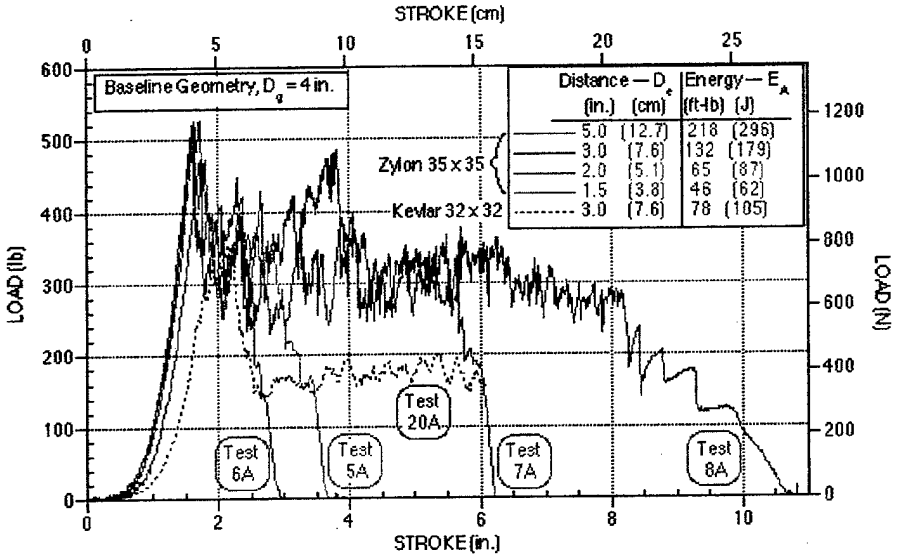

FIGURE 5. EFFECT OF HOLE-TO-FABRIC EDGE DISTANCE ON LOAD-STROKE CURVE

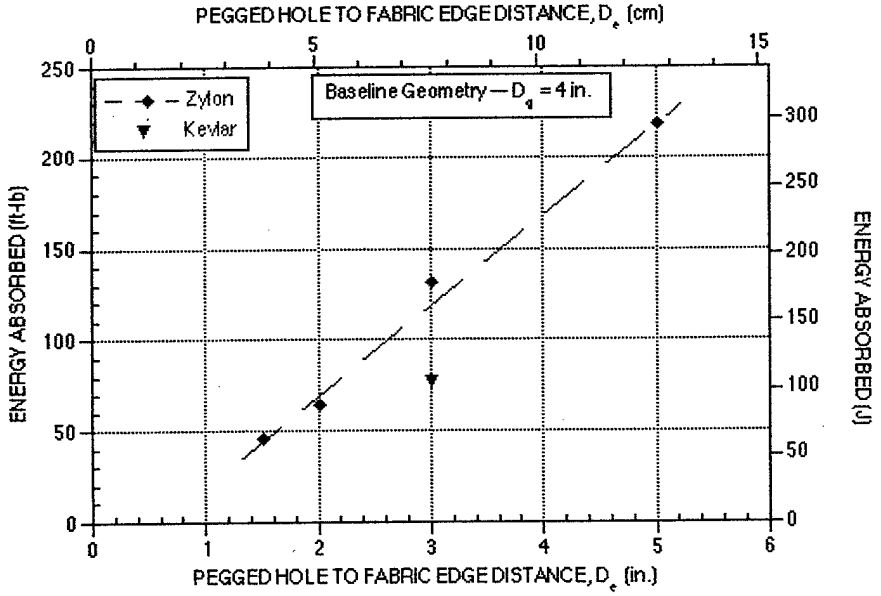

FIGURE 6. ENERGY ABSORBED AS A FUNCTION OF HOLE-TO-FABRIC EDGE DISTANCE

Other test parameters affected the energy absorbed, but much less dramatically than D_e. A 100-fold decrease in the stroke rate (from 7.5 to 0.075 in./s) did allow the material to relax and deform more between the intermittent yarn ruptures, increasing E_A somewhat, while a three-fold decrease in the peg (and hole) diameter (from 0.75 to 0.25 in.) decreased E_A slightly (see figure 7). Increasing the distance of the pegged hole from the grip (from 4 to 8.2 in.) changed the shape of the load-stroke curve somewhat (the longer the distance, the larger the stroke-to-peak load or yarn rupture initiation) but had little effect upon E_A (see figure 8). Decreasing the length of the gripped section, increasing the gap at the end of the grip, or eliminating material outside the lines perpendicular to the grip at each end had little effect upon the load-stroke curve or E_A.

For some tests, slits were cut in the fabric between the pegged hole and the corner in an attempt to guide the yarn rupture along a diagonal line toward the corner, rather than toward one edge, and to reduce the force needed to effect this rupture (this might promote failure of the fabric at the corners and retard failure in the region of impact). Typical results are illustrated in figure 9, which compares a Zylon test with and without slits. The presence of the slits reduces the initial peak load, but creates subsequent higher peak loads as the peg approaches the end of each slit.

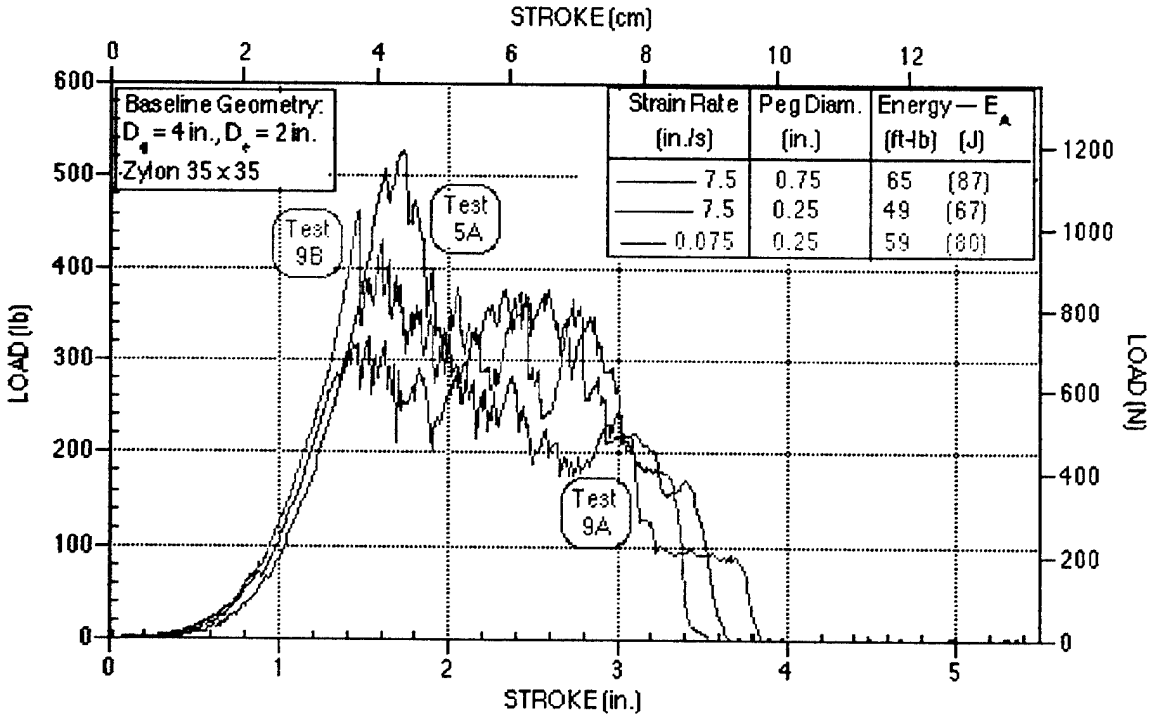

FIGURE 7. EFFECT OF STRAIN RATE AND PEG DIAMETER ON LOAD-STROKE CURVE

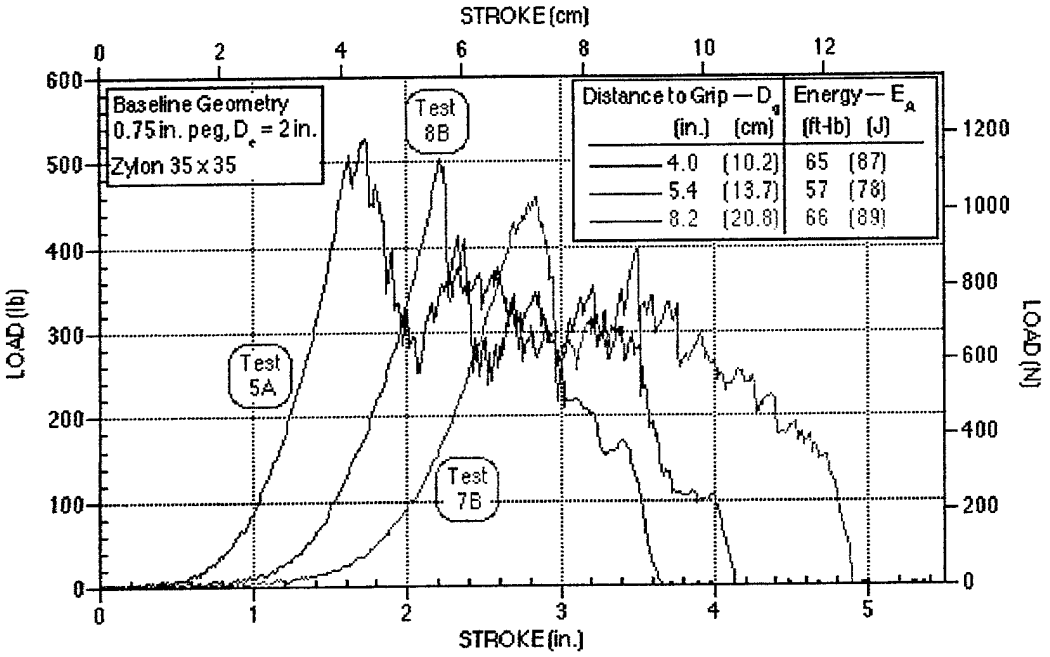

FIGURE 8. EFFECT OF DISTANCE FROM PEG TO GRIP ON LOAD-STROKE CURVE

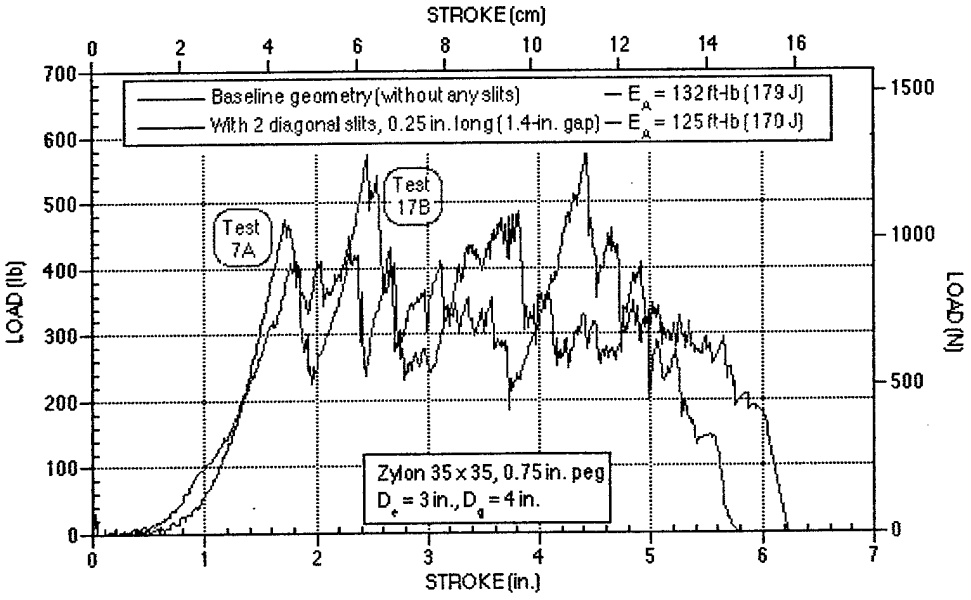

FIGURE 9. EFFECT OF SLITS IN FABRIC BETWEEN PEG AND CORNER

The total E_A is negligibly reduced. Perhaps slits that are shorter and closer together (e.g., one or two yarns each) would yield a more desirable result, but this would make the barrier very difficult and costly to produce.

A 0.5-in.-wide, heavily reinforced four-ply hem surrounded the fabric test piece for two of the tests in an attempt to prevent complete pullout of the fabric from the corner holding pegs. The hem barely prevented complete pullout—ten yarns from the hem remained intact. The hem produced a wide region of high load at large strokes, as shown in figure 10.

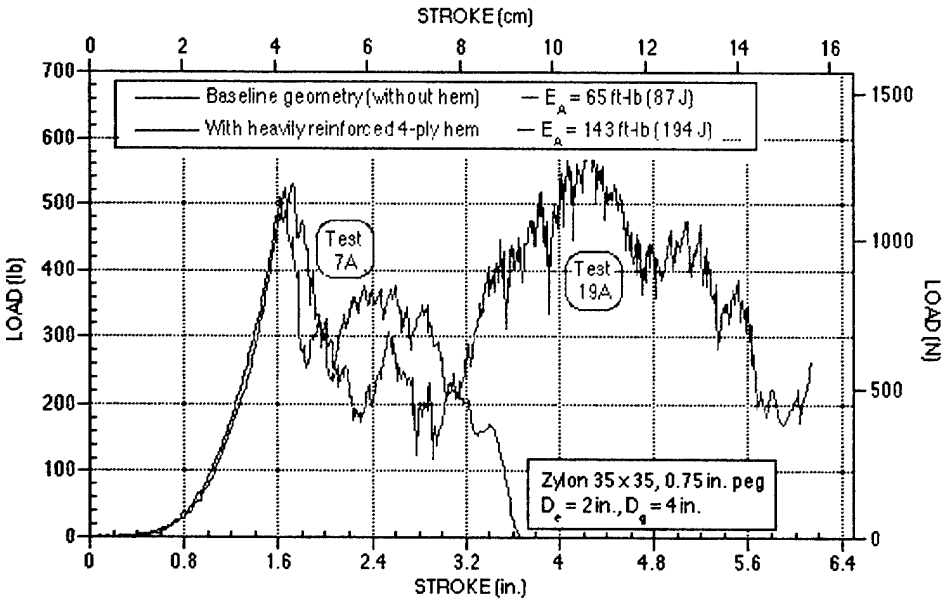

FIGURE 10. EFFECT OF HEM AROUND FABRIC TEST PIECE

DISCUSSION. When a cylindrical rod, which has been inserted through a hole near a corner of a rigidly held sheet of fabric, is displaced in the direction parallel to the plane of the fabric at about 45° to the warp and fill yarn directions, the fabric undergoes tearing from the hole outward until the tear reaches the fabric edge. The tearing occurs first by local rupture of (one or both of) the warp and fill yarns between the peg and the fabric edge, and then, when the hole is close enough to the edge (less than about 1 in., or 2.5 cm), by pullout of yarns in one direction (either warp or fill) from the other perpendicular direction.

Results of the fabric corner failure tests showed that the fabric tearing process might take considerable energy. For Zylon 35x35 fabric, once the tearing process (initial yarn rupture) begins, each additional inch (2.54 cm) of tearing, which ruptures approximately 50 yarns,* requires around 26 ft-lb (35 J) of energy. For Kevlar 32x32 fabric, the values are 15 ft-lb (20 J) to rupture 45 yarns in an inch of tearing.

In the first series of full-scale fragment impact tests, some Zylon fabric barriers underwent corner tears as long as several inches. Since a fabric barrier may contain several plies, and each ply has four corners, the total energy due to tearing may be a significant fraction of the incoming

* One inch along a 45° diagonal intersects $35/(2)^{1/2}$ warp yarns and a like number of fill yarns, for a total of 50 yarns. The tearing does not necessarily follow a 45° direction in the fabric. It usually goes along one yarn direction and then the other. On the average, the resulting number of yarn ruptures is the same as if tearing occurred along a 45° line.

fragment energy. Therefore, the fabric computational model needs to be able to handle fabric tearing around a peg.

LARGE-SCALE IMPACT TESTS AT SRI'S REMOTE TEST SITE.

SRI performed a second series of 15 large-scale fragment impact tests on the 6-in.-bore gas gun during 2001. The test configuration and procedure are presented in reference 5. The one modification made for the current series was the addition of a mirror at 45° to the direction of the camera (see figure 11) that provided a top view of the fragment. The top view, combined with the side view, allowed determination of the orientation of the fragment immediately before impact.

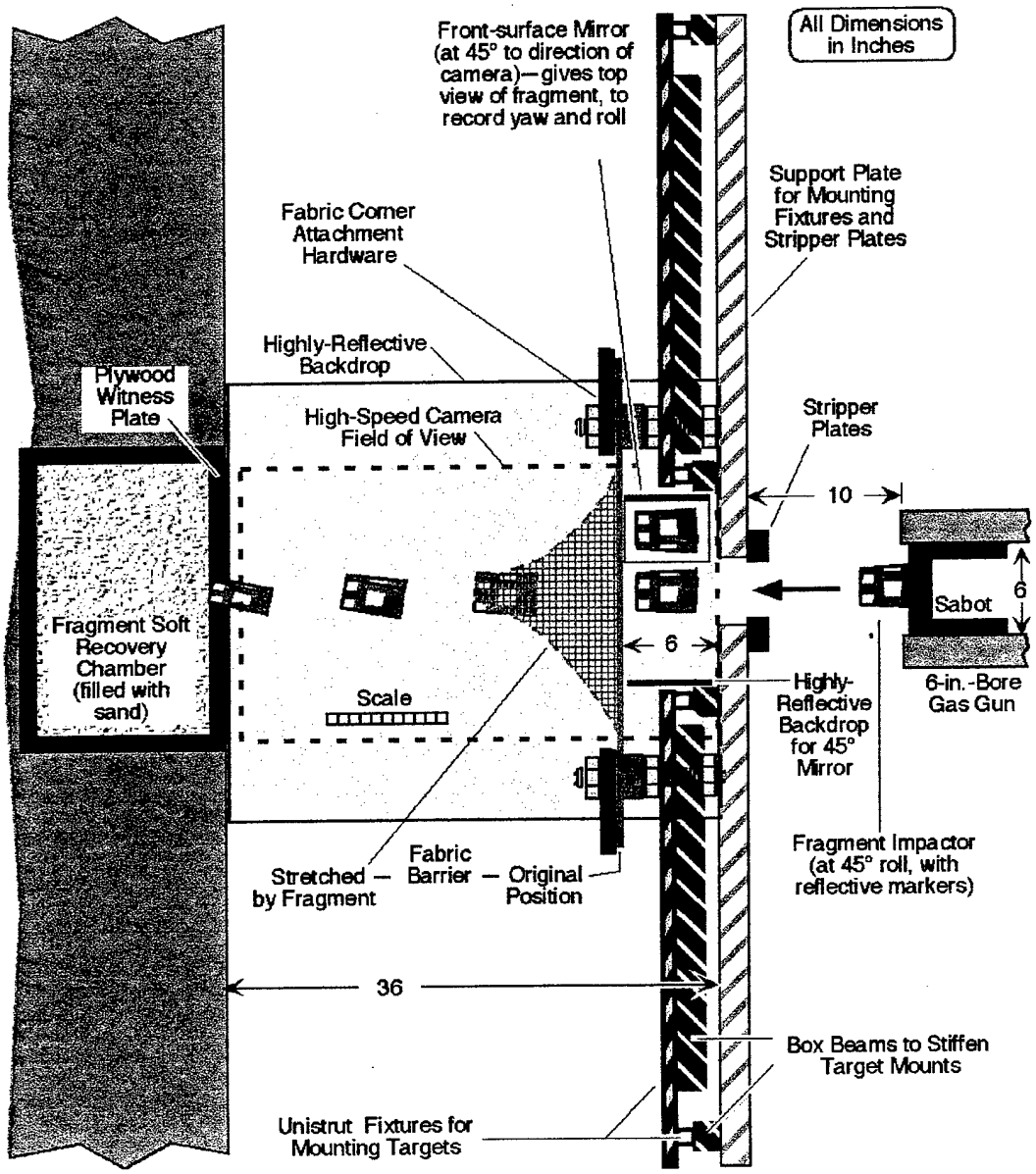

FIGURE 11. CONFIGURATION FOR THE LARGE-SCALE FRAGMENT IMPACT TESTS

TEST MATRIX. A matrix of the test parameters and results is shown in table 2. Twelve tests were performed with two to eight plies of Zylon 35x35 fabric, and three tests were performed with two plies of Kevlar 32x32 fabric. All tests were of stand-alone fabric barriers (i.e., no auxiliary materials, insulation blankets, or trim panels were present) attached to a rigid frame with pegs near the four corners. The fabric was held without slack by 1-in.-diameter pegs through holes that were placed 5 to 6 in. away from the fabric edge to reduce the likelihood of corner detachment. For all tests with Zylon, this distance was sufficient; however, for one test with Kevlar, one of the corners did detach. Therefore, on the subsequent Kevlar test, a larger distance (8.5 to 9.0 in.) was used between the pegged holes and the fabric edge, which prevented detachment.

The titanium alloy fragment impactors used in these tests were the same as those used in the first series. They were 4.0 in. (10.2 cm) long by 3.0 in. (7.6 cm) wide, and of 0.25 in. (0.62 cm) thick. The impactors tapered from the midpoint down to 0.05 in. (0.13 cm) at the impact end, where the edges were slightly rounded. They weighed about 0.40 lb (175 g).

In addition to the fabric material and number of plies, the other parameters that were varied in these tests were:

- Impact velocity — 128 to 249 m/s (420 to 815 f/s), which resulted in initial kinetic energies of 1.4 to 5.4 kJ (1.0 to 4.0 kft-lb).
- Roll angle — intended values of 0° and 45°.
- Location of impact point — either centered on the barrier or approximately halfway from the center to one of the corner-holding pegs.
- Presence of slit cuts in the fabric between the pegged hole and the fabric corner.
- Presence of an unpegged overlay as the first ply.

TEST RESULTS. Tests results shown in table 2 include the residual fragment velocity, kinetic energy absorbed by the fabric barrier, and specific energy absorbed (SEA), which equals the kinetic energy absorbed divided by the barrier's areal density. Note that for tests in which the fragment was stopped, the kinetic energy absorbed and the SEA are lower bounds to the values attainable for those barriers (except for test 120, which, as will be discussed below, was just at the ballistic limit). Also presented are the success of the barrier in stopping the fragment, the maximum axial deflection of the barrier if the fragment was stopped, the length of tearing of the fabric around the corner pegs, and the equivalent energy needed to produce this tearing (as determined by the results of the corner failure tests).

Fragment and Barrier Motion. Relevant frames from the high-speed film record of the impact tests were digitized for test analysis. Figure 12 shows an example of these frames for a test resulting in full penetration. Although the frames provide only silhouettes of the fragment and fabric barrier, the highly reflective markers placed on the fragment enable a determination of which parts of the fragment are protruding through the barrier.

TABLE 2. TEST MATRIX FOR SECOND SERIES OF LARGE-SCALE IMPACT TESTS

Test No.	Impactor[a] Mass (g) (lb)	Velocity (m/s) (f/s)	Kinetic Energy (kJ) (kft-lb)	Roll Angle (°)	Fabric Barrier[b] Material, Mesh,		Number of Plies	Areal Density (g/cm2) (lb/ft^2)	Dimensions Horiz. (cm) (in.)	Vert. (cm) (in.)	Comments (Impact point at center of fabric, except where noted)	Results: Fragment Stopped? If so, maximum axial deflection of fabric barrier (cm/in.) Corner tear dist. (cm/in.)	Residual Velocity (m/s) (f/s)	Kinetic Energy: Total Absorbed (kJ) (kft-lb)	per Ply (J) (ft-lb)	per Ply by Corner Tearing[c] (J) (ft-lb)	SEA[d] (kJ g/cm2 (kft-lb lb/ft^2
116	174	157	2.13	51	Zylon	35	2	0.0316	62.6	86.4		No	119	0.90	449	81	28.4
	0.40	513	1.57					0.0647	24.6	34.0		0.5 - 2.5 / 0.25 - 1.0	390	0.66	331	60	10.2
117	174	154	2.07	49	Zylon	35	2	0.0316	62.6	86.4	5 slits cut along diagonal	No	120	0.82	411	N.A.	26.0
	0.40	506	1.53					0.0647	24.6	34.0	be tween hole, fabric corner[e]	1.5 - 4.0 / 0.5 - 1.5	394	0.61	303		9.4
118	174	128	1.43	32	Zylon	35	2	0.0316	62.6	86.4	5 slits cut along diagonal	Yes — 34/13.5	0	> 1.43	> 715	N.A.	> 45.2
	0.40	420	1.05					0.0647	24.6	34.0	between hole, fabric corner[e]	4.0 - 7.5 / 1.5 - 3.0	0	> 1.05	> 527		> 16.3
119	174	132	1.52	29	Zylon	35	2	0.0316	62.6	86.4		No	66	1.13	566	167	35.8
	0.40	433	1.12					0.0647	24.6	34.0		1.5 - 5.0 / 0.5 - 2.0	218	0.84	418	123	12.9
120	174	183	2.91	45	Zylon	35	4	0.0632	62.6	86.4	7 slits cut along diagonal	Yes[f] — 39/15.5	0	2.91	728	N.A.	46.1
	0.40	600	2.15					0.1294	24.6	34.0	between hole, fabric corner[e]	2.5 - 6.5 / 1.0 - 2.5	0	2.15	537		16.6
121	176	177	2.74	48	Zylon	35	4	0.0632	62.6	86.4		Yes — 32/12.5	0	> 2.74	> 686	315	> 43.4
	0.40	579	2.02					0.1294	24.6	34.0		4.0 - 7.5 / 1.5 - 3.0	0	> 2.02	> 506	233	> 15.6
122	176	128	1.44	13	Zylon	35	2	0.0316	62.5	81.9	Intended 0° Roll	Yes — 33/13	0	> 1.44	> 718	349	> 45.4
	0.40	419	1.06					0.0647	24.6	32.3		5.0 - 6.5 / 2.0 - 2.5	0	> 1.06	> 529	257	> 16.4
123	176	249	5.43	33	Zylon	35	8	0.1264	62.5	81.9		No	79	4.89	611	233	38.7
	0.40	815	4.01					0.2589	24.6	32.3		3.0 - 5.0 / 1.25 - 2.0	257	3.61	451	172	13.9
124	176	100	0.87	32	Kevlar	32	2	0.0224	62.5	81.9		Yes — 36/14	0	> 0.87	> 436	244	> 38.9
	0.40	326	0.64					0.0459	24.6	32.3		7.5 - 11.5/ 3.0 - 4.5	0	> 0.64	> 321	180	> 14.0
125	176	128	1.44	52	Kevlar	32	2	0.0224	62.5	81.9	Complete detachment of	Yes — N.A.	0	> 1.44	> 718	361	> 64.1
	0.40	419	1.06					0.0459	24.6	32.3	peg from barrier in 1 corner	5.0 - 12.5 / 2.0 - 5.0	0	> 1.06	> 529	267	> 23.1
126	176	182	2.91	42	Zylon	35	4	0.0632	62.5	81.9	1st ply—unpegged overlay	No (Overlay unperforated)	57	2.62	656	293	41.5
	0.40	596	2.15					0.1294	24.6	32.3	16.5 x 24.5 in. (horiz./vert.)	5.0 - 6.5 / 2.0 - 2.5	187	1.93	484	216	14.9
127	174	230	4.61	52	Zylon	35	8	0.1264	62.5	81.9		No	124	3.28	410	67	25.9
	0.40	755	3.40					0.2589	24.6	32.3		0.0 - 2.5 / 0.0 - 1.0	407	2.42	302	50	9.3
128	176	136	1.63	36	Kevlar	32	2	0.0224	81.3	100.3	8.5 - 9 in. of fabric extended	Yes — 46/18	0	> 1.63	> 817	405	> 73.0
	0.40	447	1.21					0.0459	32.0	39.5	from peg to barrier edges	7.5 - 15.0 / 3.0 - 6.0	0	> 1.21	> 603	299	> 26.3
129	174	217	4.10	31	Zylon	35	8	0.1264	62.5	81.9		Yes — 30/12	0	> 4.10	> 512	188	> 32.4
	0.40	712	3.02					0.2589	24.6	32.3		1.5 - 4.5 / 0.5 - 1.75	0	> 3.02	> 378	138	> 11.7
130	176	127	1.41	43	Zylon	35	2	0.0316	62.5	81.9	Impact 5.5 in. above, 3 in.	No	93	0.65	325	48	20.5
	0.40	415	1.04					0.0647	24.6	32.3	to left of barrier center	0.5 - 3.0 / 0.25 - 1.25	305	0.48	239	35	7.4

[a] All tests had 0° ± 1° pitch, 0° ± 3° yaw and impact obliquity; intended roll was 45° except where noted; roll angle values are ± 2°.

[b] Barriers are held without slack by four 1-in.-diameter pegs through holes in the fabric whose centers are 21.25 in. apart vertically and 13 in. apart horizontally. Pegs are centered within the barrier, with ≈5-6 in. of material between peg and edge, except where noted.

[c] As calculated using results of fabric corner failure tests: 35 J (26 ft-lb) per in. of tear for Zylon 35 x 35, 20 J (15 ft-lb) per in. for Kevlar 32 x 32.

[d] Specific Energy Absorbed (SEA) — kinetic energy absorbed divided by areal density; for tests where the fragment was stopped, the SEA is a lower bound.

[e] Slits are ≈0.35 in. (0.89 cm) long, are separated by a distance equal to their length, and begin at the same distance beyond the pegged hole.

[f] Fragment completely perforated fabric barrier, but ended up with a very slightly negative residual velocity.

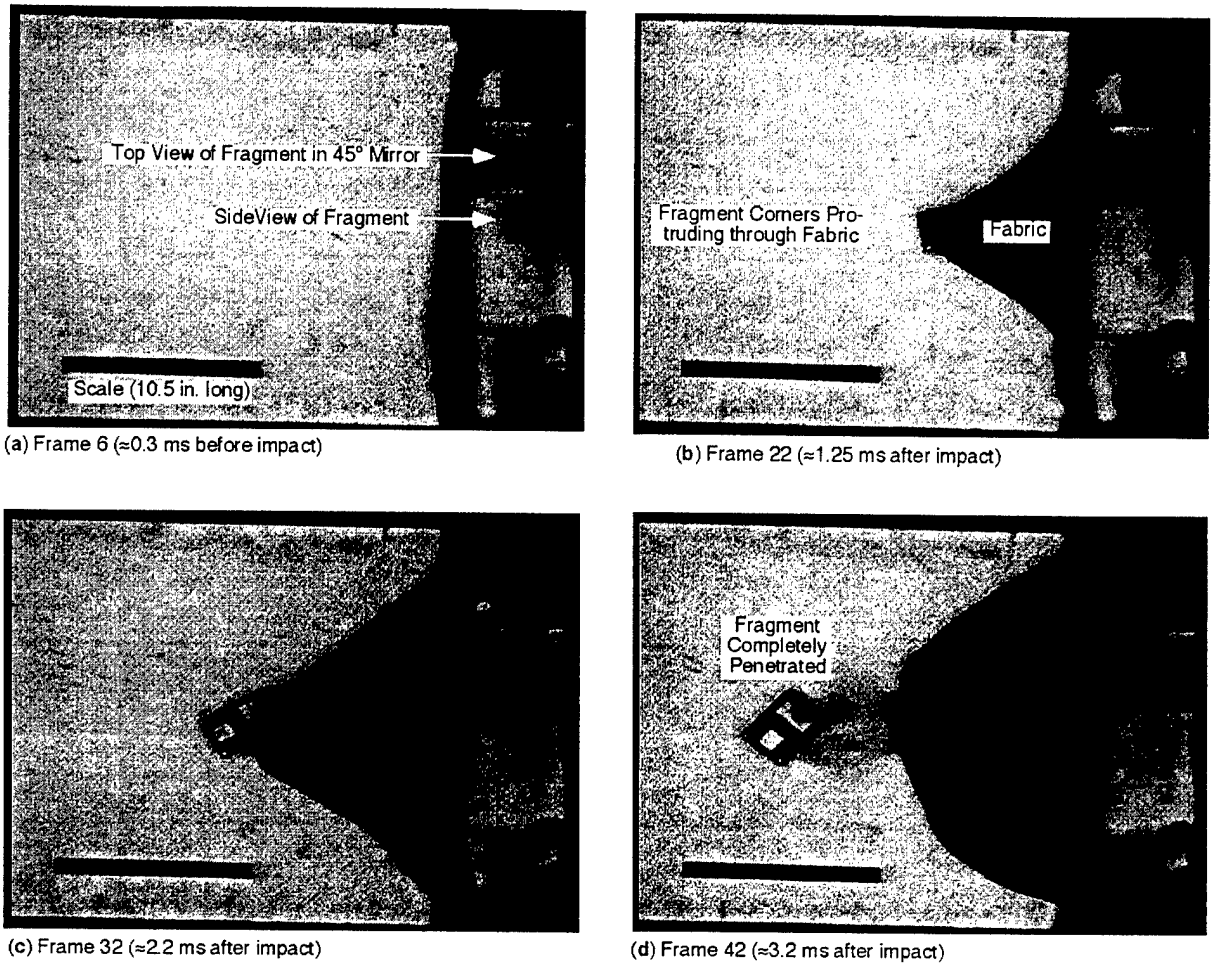

(a) Frame 6 (≈0.3 ms before impact)

(b) Frame 22 (≈1.25 ms after impact)

(c) Frame 32 (≈2.2 ms after impact)

(d) Frame 42 (≈3.2 ms after impact)

FIGURE 12. SELECTED FRAMES FROM CAMERA RECORD OF TEST 127
(at 10,370 frames/s)

Examination of the film records revealed that yaw, pitch, and impact obliquity were all within their measurement uncertainties (±1° for pitch and ±2° for yaw and obliquity) of their intended values. Roll varied by more than the measurement uncertainty (±2°), but since no fragment rotation was seen during the fragment's 6 in. travel before impact, the roll was likely due to rotation of the sabot during emplacement in the gas gun breech. The difference between the measured and intended roll values averaged only ≈ 7°.

The digitized records are used to obtain the velocity and orientation history of the fragment and the deformation history of the fabric barrier. This data is put into graphical form and made available for comparison with the computational simulations for model refinement and validation. The next 12 figures give examples of these graphs for a range of penetration results.

As an example of a test resulting in complete penetration, figure 13 shows silhouettes of the fragment and the downstream edge of the fabric at various times before impact and during and after penetration in test 127. The front corners of the fragment penetrated the barrier at relatively early times after impact (by frame 16), the fragment began to rotate, and then broke free of the barrier between frames 31 and 36. Figures 14 and 15 show the axial position and

velocity histories for this test. The position curves appear quite smooth, but the velocity curves are jagged. Although the positions in the digitized film frame can be read to within ±1 pixel, a 1-pixel change in location of a point on the digitized frame can lead to as large as a 13 m/s change in velocity between subsequent frames. The initial and residual velocities, are therefore, calculated as the average over many frames. Also, since the fragment has a residual rotation after penetration, the final velocities of the four fragment corners are not the same (and are not constant). The final velocity was taken as the average of all four corners after separation from the barrier.

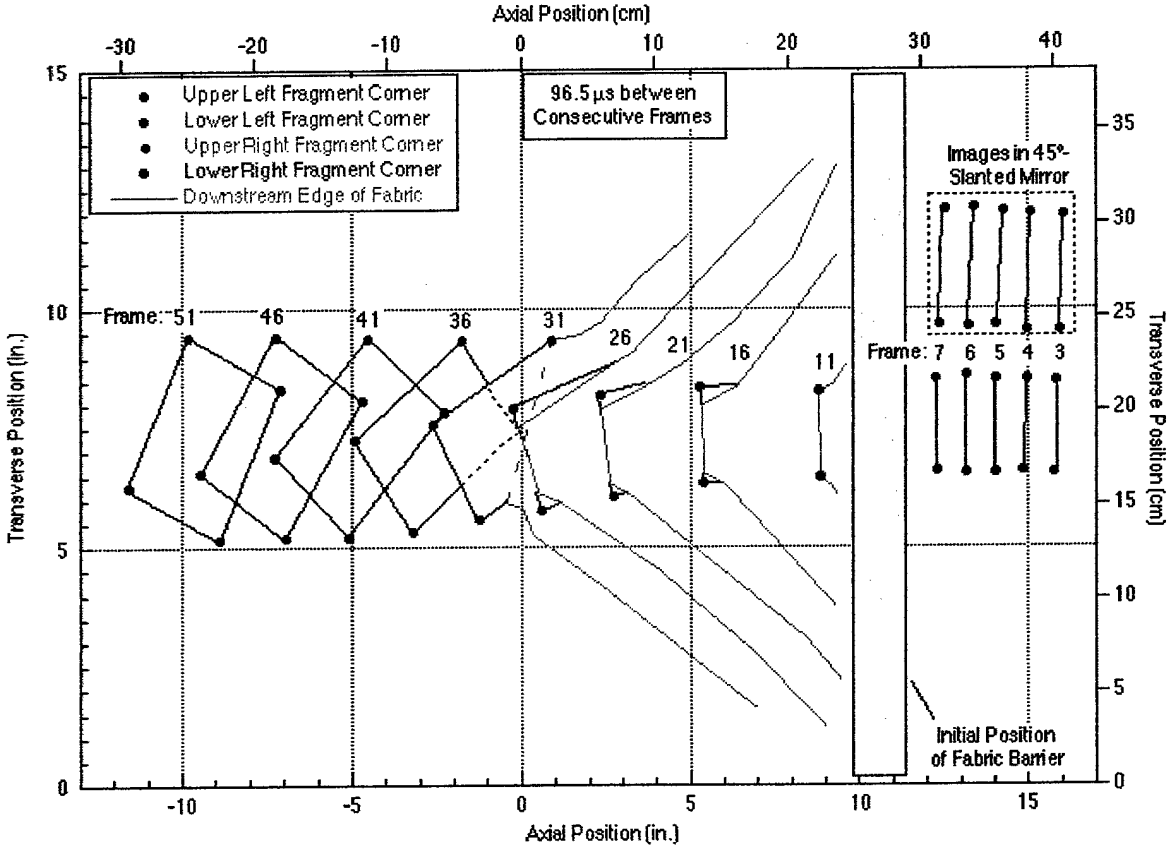

FIGURE 13. SILHOUETTES OF FRAGMENT MOTION AND FABRIC DEFORMATION FOR TEST 127

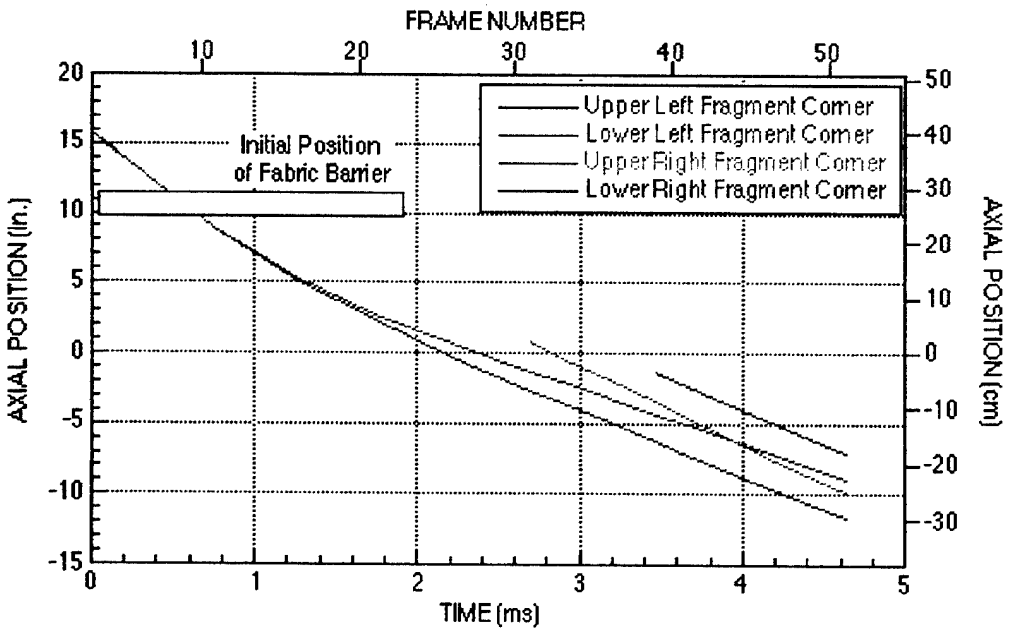

FIGURE 14. AXIAL POSITION OF FRAGMENT CORNERS FOR TEST 127

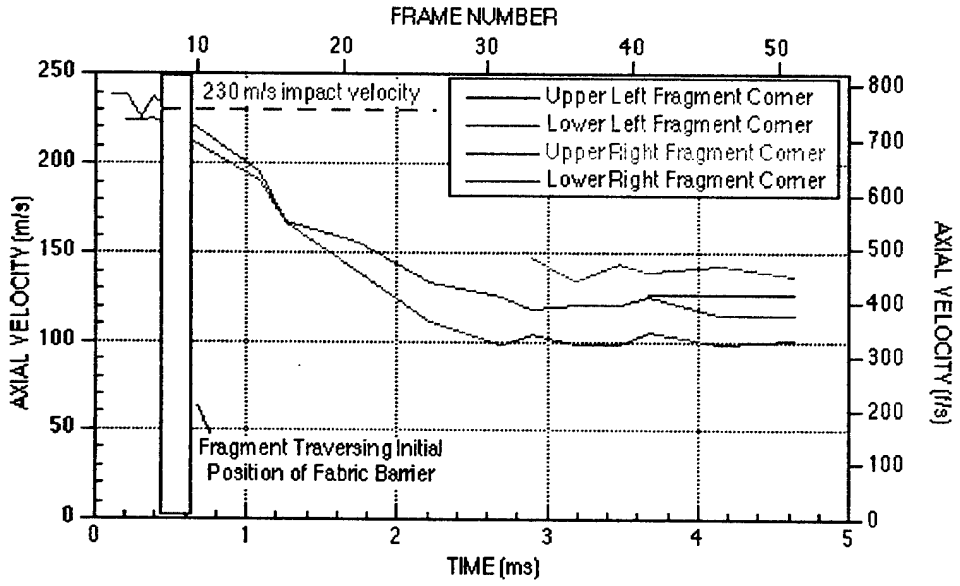

FIGURE 15. AXIAL VELOCITY OF FRAGMENT CORNERS FOR TEST 127

As an example of a test resulting in no penetration, figure 16 shows the fragment and fabric silhouettes for test 121. Axial position and velocity histories are shown in figures 17 and 18, respectively. Although the front corners of the fragment perforated the fabric slightly (not shown in the figure), the barrier did not allow complete penetration. The fragment rotated completely so that the back edges of the fragment are seen pushing against the fabric during the last dozen or so frames before the barrier's maximum deformation.

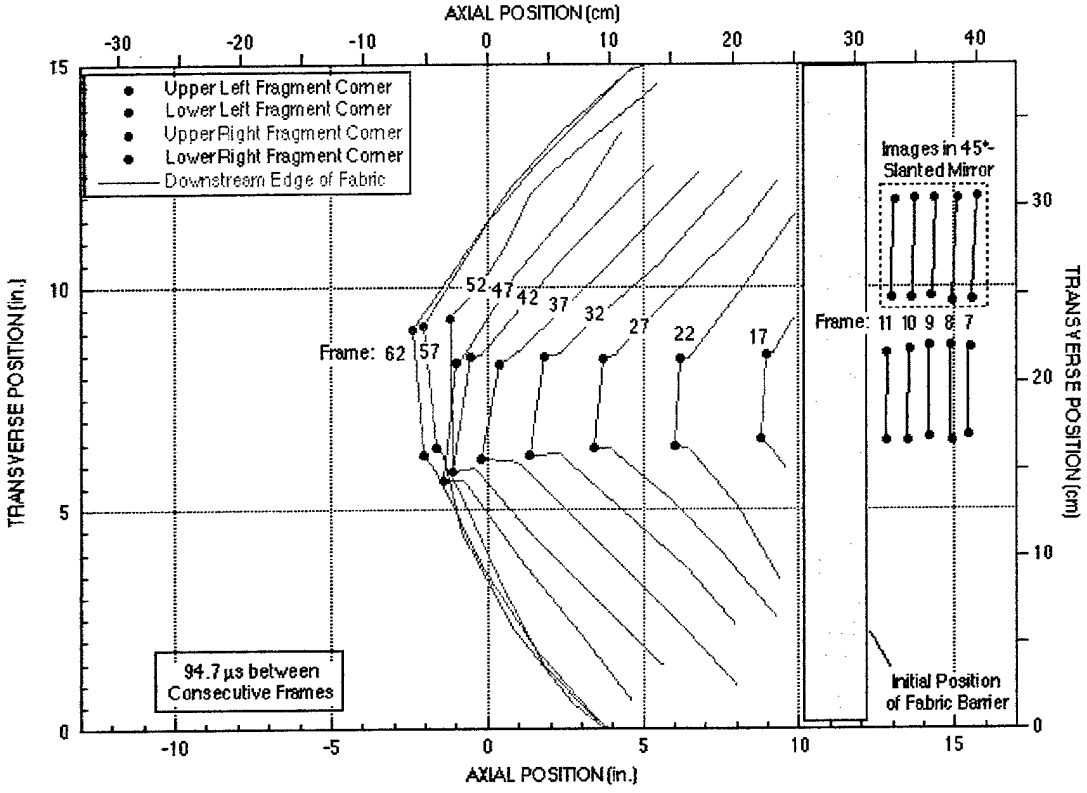

FIGURE 16. SILHOUETTES OF FRAGMENT MOTION AND FABRIC DEFORMATION FOR TEST 121

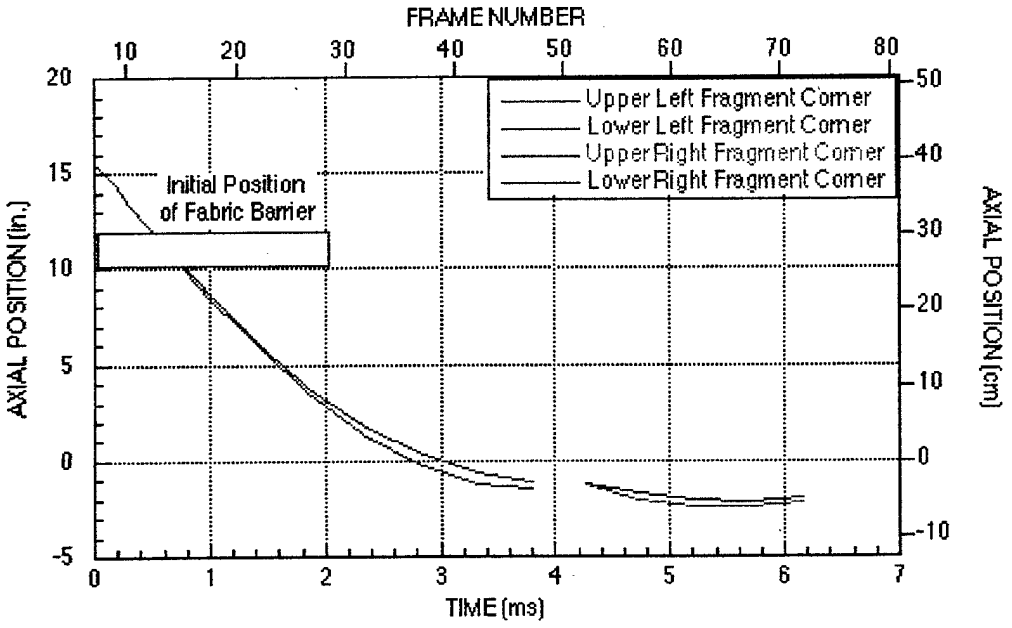

FIGURE 17. AXIAL POSITIONS OF FRAGMENT CORNERS FOR TEST 121

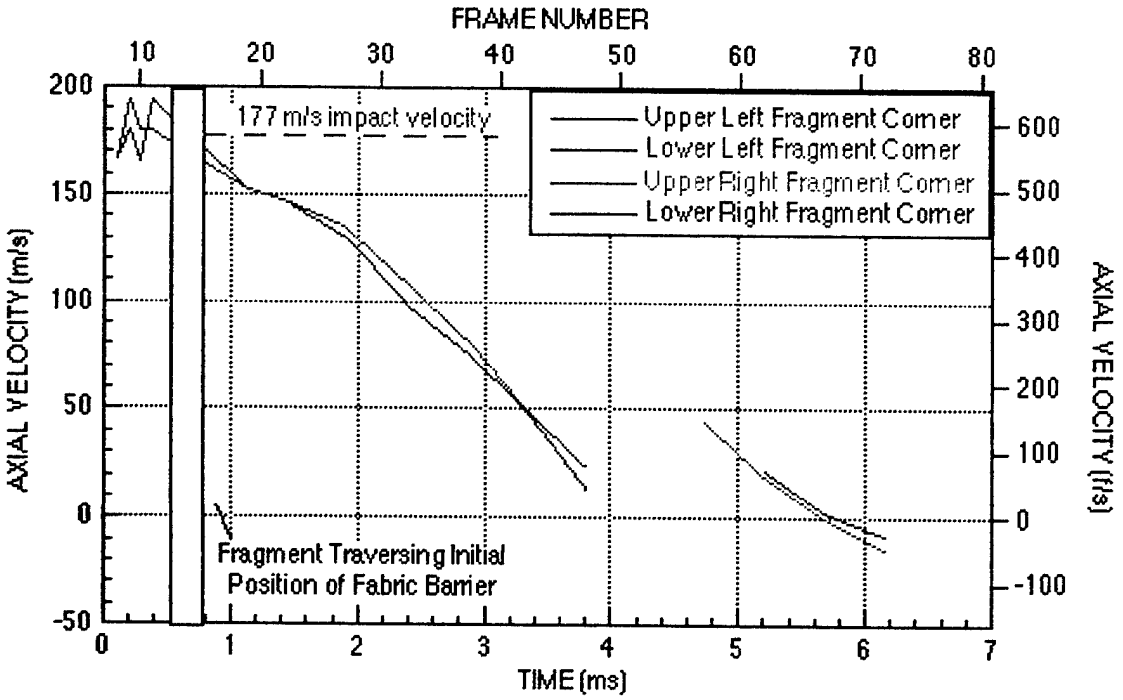

FIGURE 18. AXIAL VELOCITY OF FRAGMENT CORNERS FOR TEST 121

As an example of a test at the ballistic limit of the barrier, figure 19 shows the fragment and fabric silhouettes for test 120, while figures 20 and 21 show the axial position and velocity histories. The fragment completely perforated the barrier (after frame 58, the barrier began to retract toward its initial position) and ended up on the downstream side of the barrier (completely separate after about frame 103). But the last few yarns in contact with the fragment exerted sufficient pull so that the fragment ended up with a slightly negative residual velocity.

The last example is a test of an ungripped fabric overlay used as the first barrier ply. Figure 22 shows the fragment and fabric silhouettes for test 126, while figures 23 and 24 show the axial position and velocity histories. The fragment completely perforated the three gripped plies, but not the overlay. The fragment, cloaked inside the overlay, broke through the barrier at around frame 50 and continued to decelerate slightly until the entire overlay had squeezed through the hole in the gripped plies (around frame 80).

Energy Absorption. The energy absorption and areal density values for the fragment impact tests are plotted in figure 25. Figure 25 included all the tests from the second series, shown in table 3, except one test (test 125) that resulted in a corner detachment, and the three stand-alone fabric barrier tests from the earlier large-scale impact test series [5], which resulted in no corner detachment.

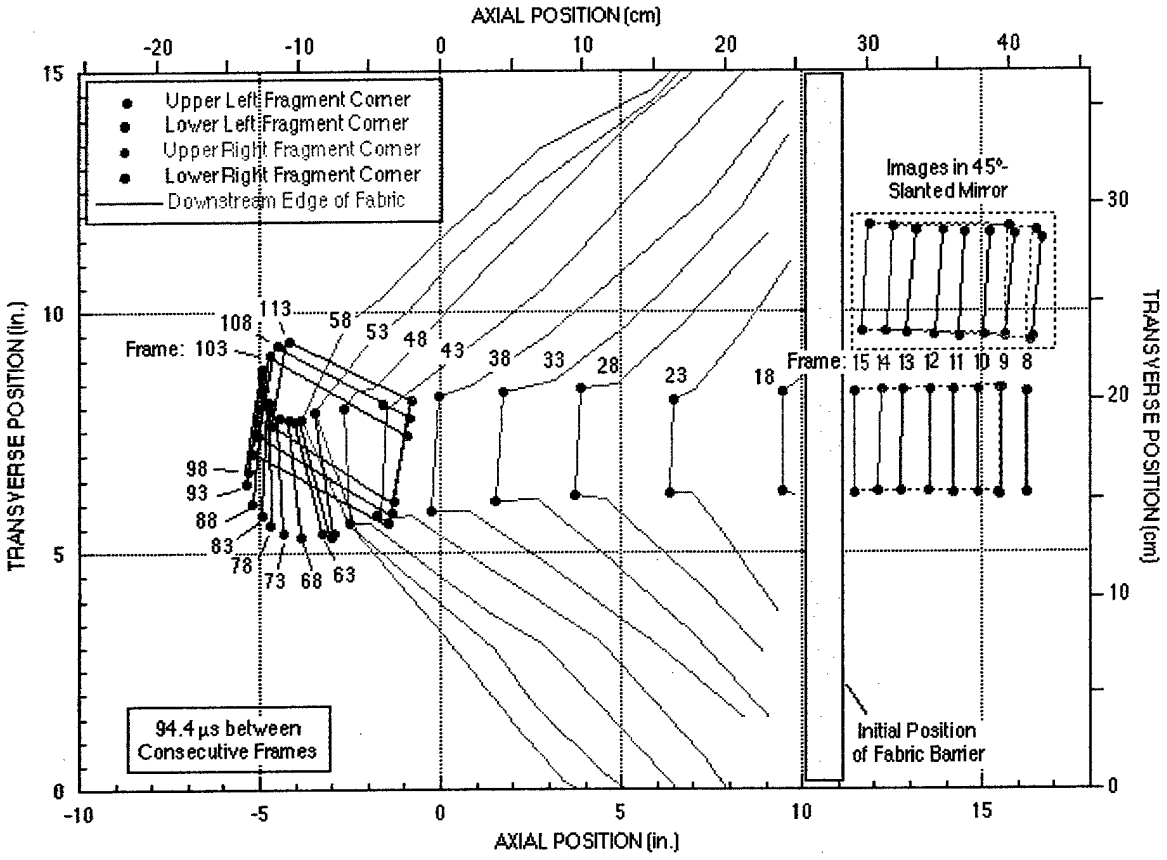

FIGURE 19. SILHOUETTES OF FRAGMENT MOTION AND FABRIC DEFORMATION FOR TEST 120

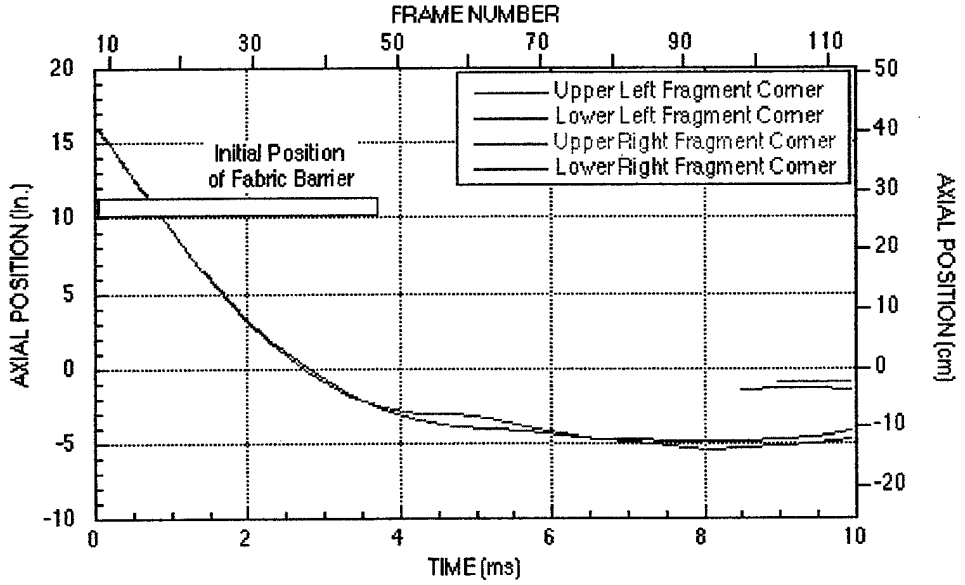

FIGURE 20. AXIAL POSITIONS OF FRAGMENT CORNERS FOR TEST 120

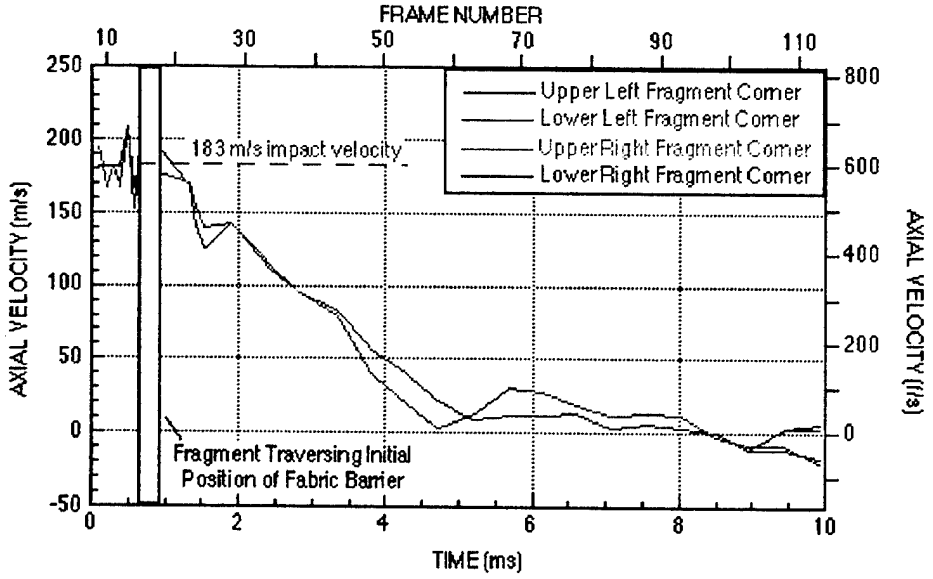

FIGURE 21. AXIAL VELOCITY OF FRAGMENT CORNERS FOR TEST 120

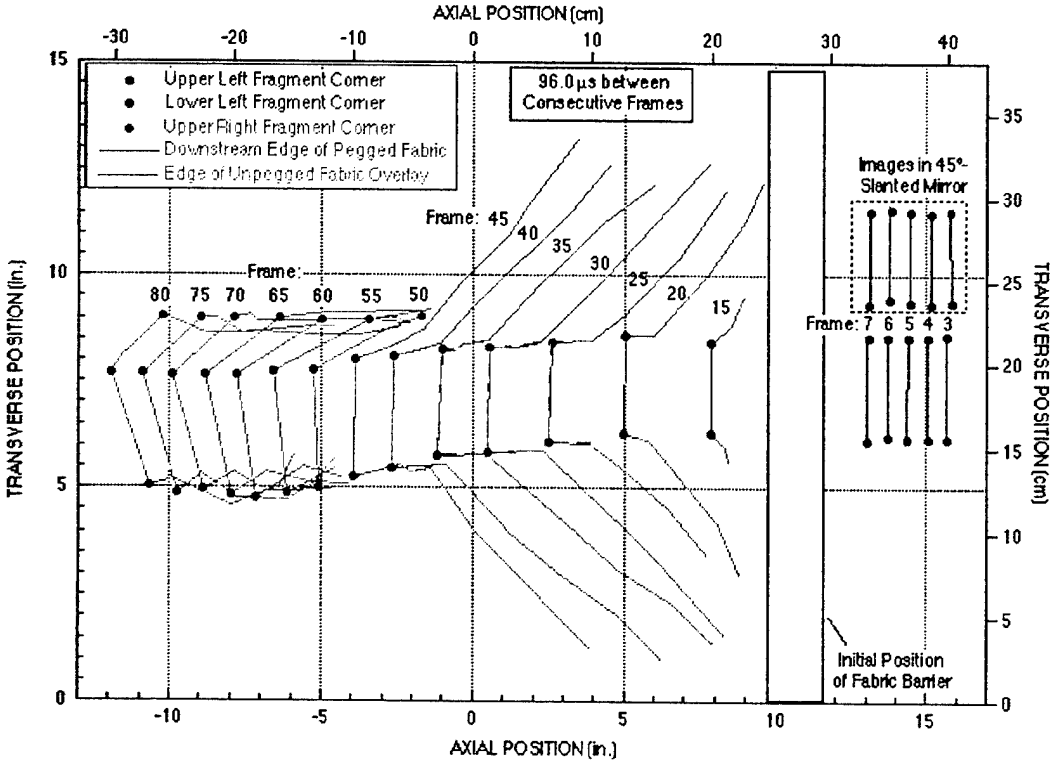

FIGURE 22. SILHOUETTES OF FRAGMENT MOTION AND FABRIC DEFORMATION FOR TEST 126

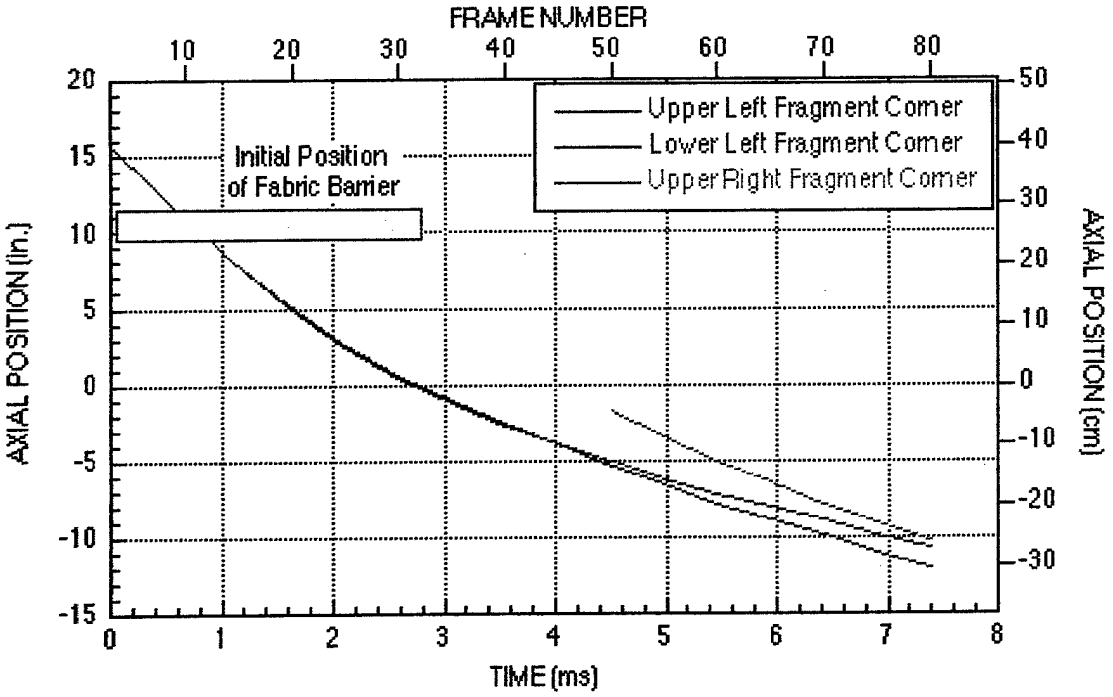

FIGURE 23. AXIAL POSITIONS OF FRAGMENT CORNERS FOR TEST 126

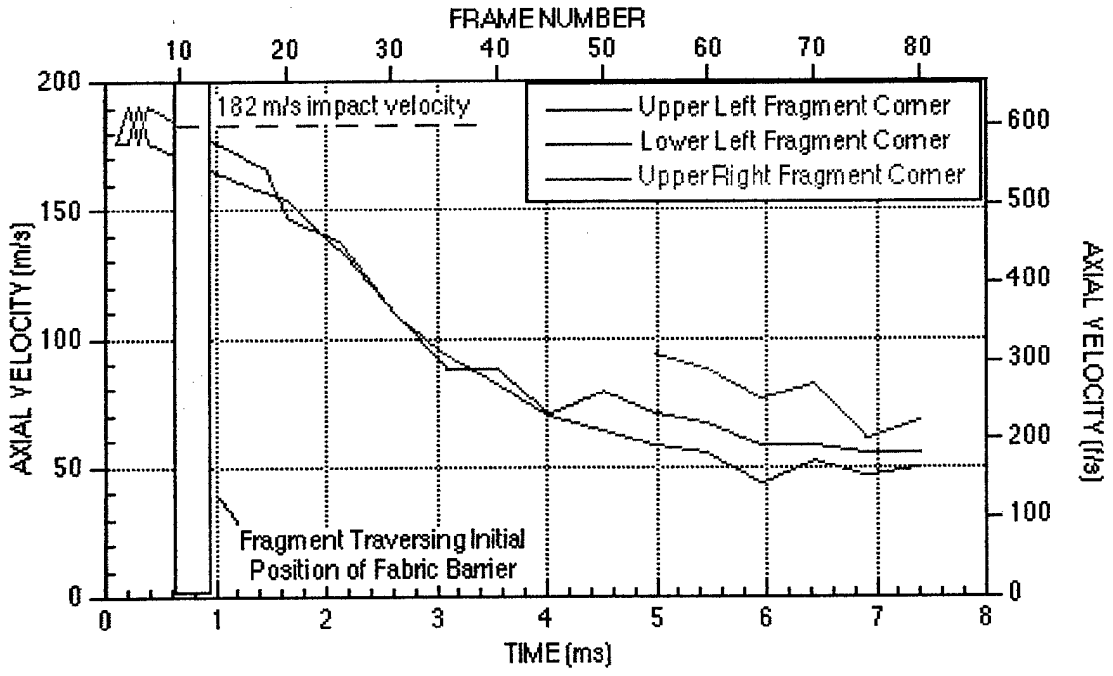

FIGURE 24. AXIAL VELOCITY OF FRAGMENT CORNERS FOR TEST 126

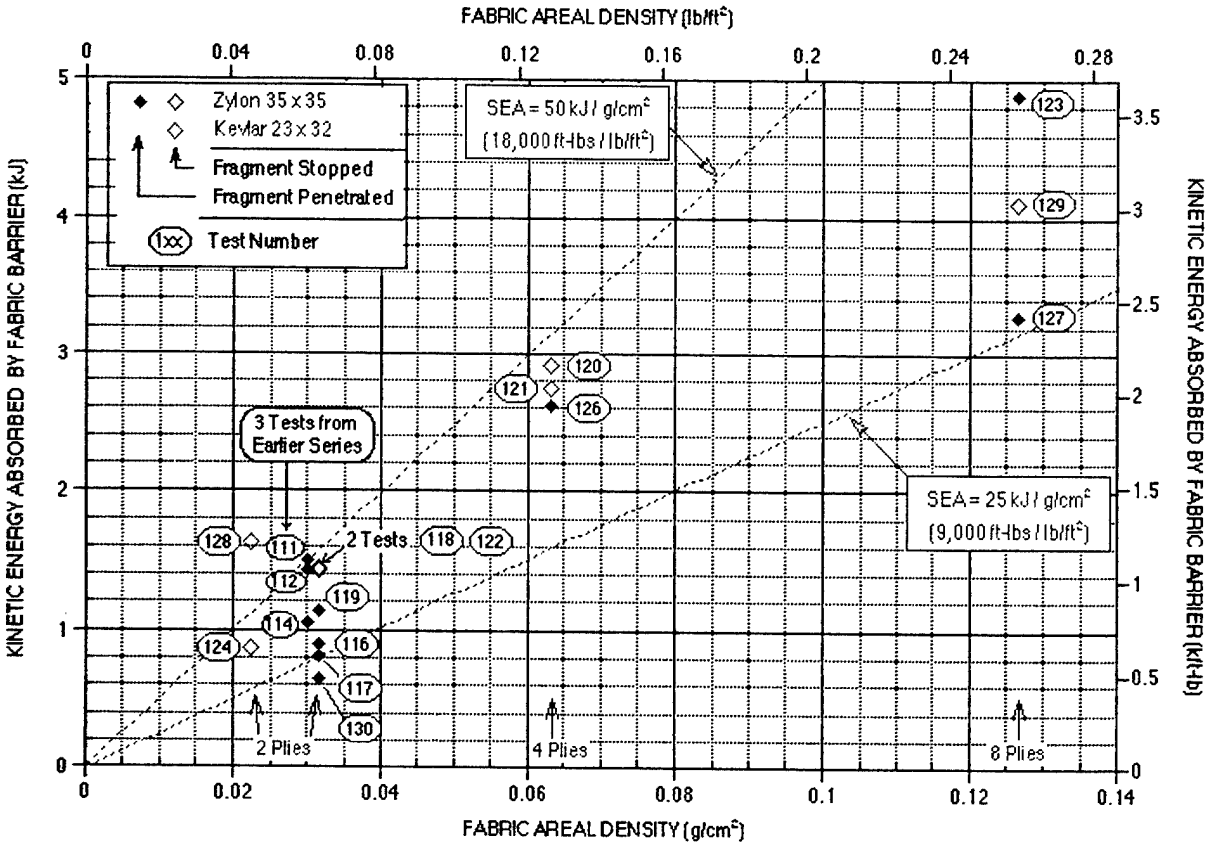

FIGURE 25. KINETIC ENERGY ABSORBED AS A FUNCTION OF FABRIC AREAL DENSITY FOR IMPACT TESTS

TABLE 3. HIGH-STRENGTH WOVEN FABRIC MATERIALS

Trade Name[a]		Zylon-AS			Kevlar-29
Material		PBO (polybenzobisoxazole)			P-Aramid
Volume Density	(g/cm^3)	1.54			1.44
Nominal Yarn Denier[b]		500			400
Mesh	(yarns/in)	30x30	35x35	40x40	32x32
Thickness	(in)	0.006	0.007	0.009	0.007
	(mm)	0.15	0.19	0.23	0.18
Areal Density	(g/cm^2)	0.013	0.0158	0.0185	0.113
	(lb/ft^2)	0.0266	0.0324	0.0378	0.0232

[a] Zylon was supplied by Toyoba Co., Ltd., Osaka, Japan; Kevlar was obtained from Fabric Development Inc., Quakertown, PA
[b] Denier denotes linear density of yarns in terms of grams per 9 kilometers. Actual values varied by ±10% from nominal values.

The SEA results for the Zylon barriers were, with one exception to be noted below, all within the range of 25 to 50 kJ/g/cm^2 (9 to 18 kft-lb/lb/ft^2). The energy absorbed appears to be proportional to the number of plies for tests with two and four plies. The ballistic limit is close to an SEA of 45 kJ/g/cm^2 (16 kft-lb/lb/ft^2). The energy absorbed per ply decreases somewhat for the tests with eight plies; there is a larger degree of scatter for those three tests.

As expected from the corner failure tests, the slits cut in the fabric between the pegged hole and the fabric corner did not have much effect upon the fabric barrier energy absorption results (compare, for example, test 116 with 117 and test 120 with 121). Variation of the roll angle (measured values were between 13° and 52°) also did not have any significant effect on the energy absorption (compare tests 122 and 118).

Having an unpegged overlay as the barrier's first fabric ply did not improve the performance of the barrier compared with all of the plies being pegged (compare tests 126 and 121). The overlay worked as desired, in that it was not perforated but the fragment, encased in the overlay, penetrated the remainder of the barrier. Therefore, the additional energy absorbed by deforming and accelerating the overlay and by dragging the overlay through the remaining plies was less than that of stretching and perforating an additional pegged ply.

The one parameter that did have a noticeable effect upon the barrier's energy absorption was the location of the impact point. When a fragment hit midway between the fabric's midpoint and one of the four corner pegs, the resultant SEA was only 20.5 kJ/g/cm^2 (7.4 kft-lb/lb/ft^2). This value was 60% of the SEA when the fragment hit at the midpoint (compare tests 130 and 119).

The SEAs of the Kevlar barriers ranged from 39 to as high as 73 kJ/g/cm^2 (14 to 26 kft-lb/lb/ft^2). This high value (from test 128) was surprising, in that Kevlar had consistently performed well below Zylon (in terms of SEA) in all of the tests in which the fabric was tightly gripped on two or four sides. An important factor in this unexpected effectiveness of Kevlar barriers in the corner-pegged fabric holding geometry is the relative ease and degree of corner tearing. The corner failure tests showed that it took about 40% less energy to create a tear around a cylindrical peg in Kevlar than it did to create a tear of the same length in Zylon. Examination of the recovered fabric barriers from the impact tests showed significantly longer tears in Kevlar than in Zylon for tests with similar impact velocities and number of plies (see figure 26). The increased corner tear lengths also led to increased maximum axial deflection of the barrier before stopping the fragment—as large as 46 cm (18 in.) for Kevlar compared with 34 cm (13.5 in.) for Zylon.

Figure 27 graphs the energy used, per ply, to produce the tearing in the fabric around the corner pegs (based on results of the corner failure tests) versus the total energy absorbed by the fabric. In the tests for which the fragment was stopped, usually a larger fraction of the energy was used in creating corner tears, as compared with tests that resulted in fragment penetration. Kevlar, in fact, used ≥ 50% of the total energy absorbed to create corner tearing while preventing fragment penetration. Figure 27 shows the significant fraction of energy used in corner tearing, and, hence, the importance of this phenomenon in the penetration results.

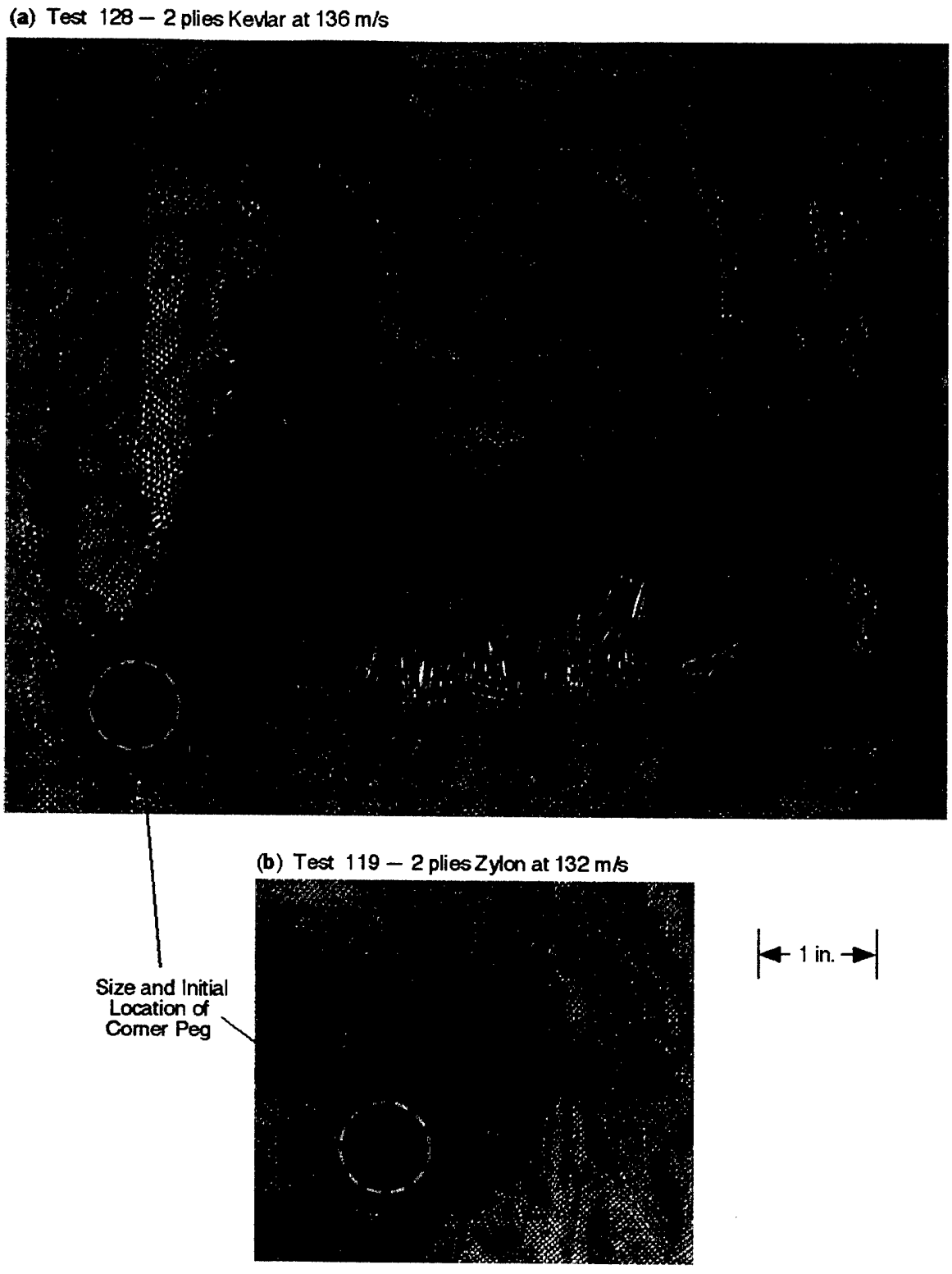

FIGURE 26. CORNER TEARING DAMAGE IN TWO FABRIC BARRIER IMPACT TESTS

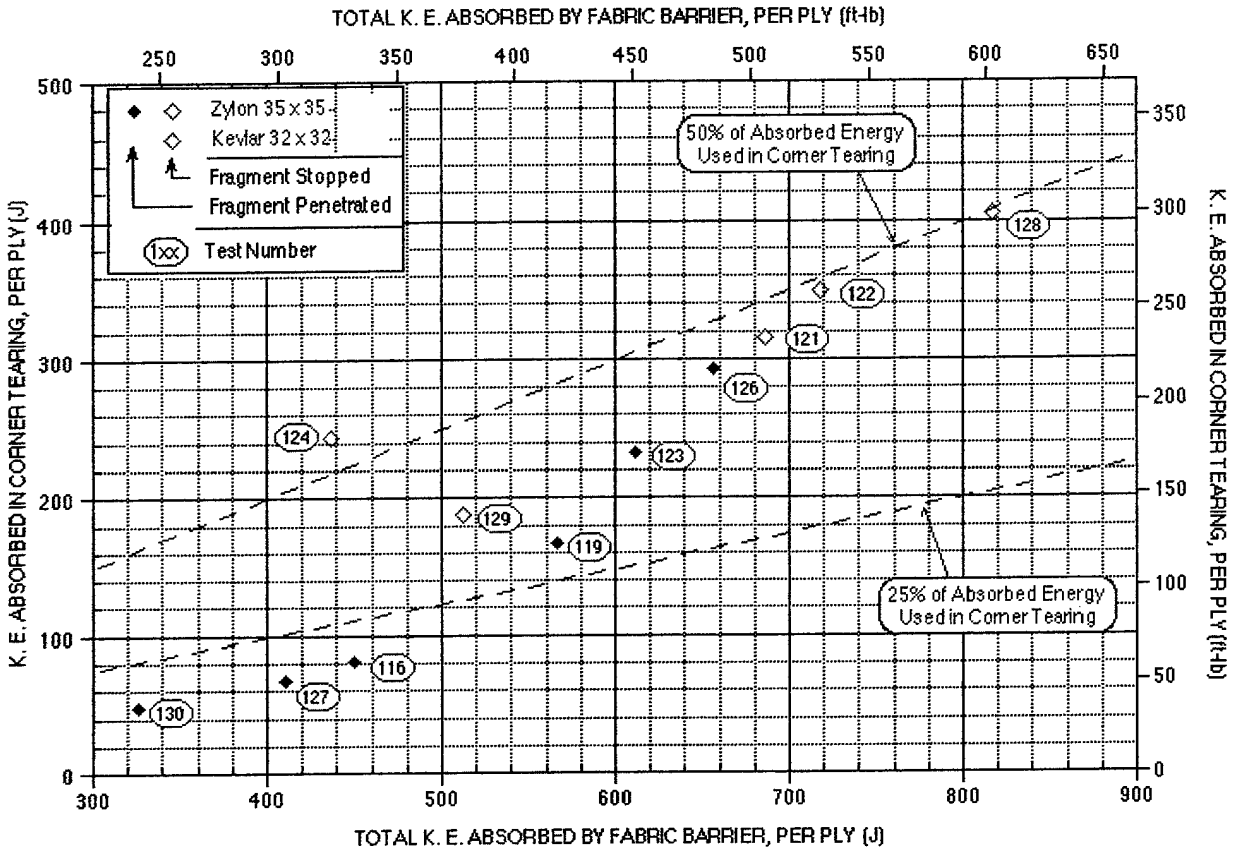

FIGURE 27. KINETIC ENERGY ABSORBED IN CORNER TEARING VERSUS TOTAL ENERGY ABSORBED

DISCUSSION. A considerable database from large-scale fragment impact tests into stand-alone Zylon and Kevlar fabric ballistic barriers is now available for the purpose of fabric computational model refinement and verification.

For fabric barriers held with pegs near the corners, Kevlar may be as effective a barrier as Zylon because of its tendency to tear around the pegs. However, it may be that pegs may not be the fastening of choice for aircraft applications. The corner failure tests have shown that the force applied to the mounting peg by the fabric can be considerable—a peak of 500 lb (2200 N), followed by a 310 lb (1380 N) plateau for one ply of Zylon. For eight plies, the force would peak at 4000 lb (17,600 N) and plateau at 2480 lb (11,040 N) for each corner peg. This force was sufficient to cause significant bending in the 1/2-in.-diameter threaded rods used to attach the pegs to the mounting frame in the fragment impact tests. The force on the attachment hardware needs to be measured, and the effect of this force on the fuselage structure to which it is attached, as well as the weight of the hardware needed to resist this force should to be considered in designing fragment barriers for aircraft.

COMPUTATIONAL MODELING OF FABRIC BARRIERS

DEVELOPMENT OF DESIGN MODEL FOR ZYLON FABRIC.

As described in previous reports [3 and 5], a simplified finite element fabric model is being developed to be used as a design tool for choosing or evaluating parameters for fragment barriers. The design tool uses a continuum description of the fabric. The calculations run quickly (about 10 minutes for a 3000-element simulation of a gas gun test using six processors on a Linux cluster) and easily allows evaluation of changes in size of fabric, number of layers, or method of attachment.

This report investigates the reliability of the design model by performing calculations with a single set of material properties to simulate a range of tests, including push tests, laboratory gas gun tests, and large-scale impact tests. A single material, Zylon 35x35, was used for the chosen set of experiments.

REQUIREMENTS. The requirements for an engineering design model based on results of the experiments are to match the following response quantities of the fabric.

- Force-displacement response. In quasi-static push tests when fabric is gripped on two edges or gripped on four edges. In the large-scale impact tests, fabric position and fragment velocity, as the barrier is deformed.

- Residual velocity in dynamic tests. In both the gas gun tests and the large-scale tests, the residual velocity of the fragment is the best measurement of the barrier's effectiveness.

- Damage response in static and dynamic tests. In all tests, much of the damage in the fabrics tends to be localized around the fragment; no excessive ripping occurs. In push tests with gripping on two sides, damage also occurs at a distance from the fragment. In the large-scale tests, the fabric rips at the attachments.

Results from the push tests were used to get constitutive and failure properties for the fabric. An attempt was made to get a good overall match with all the test results. In general, it was found that the model tends to overpredict the strength of fabric gripped on four sides and to slightly underpredict the strength of fabric gripped on two sides.

CONSTITUTIVE MODEL. The constitutive model is orthotropic with high tensile stiffness in the yarn direction. The fabric is assumed to be elastic-plastic with linear hardening in the two orthogonal directions. For a single layer of 35x35 Zylon, the tensile modulus was selected to be 4.2×10^{11} dyne/cm^2 as determined from push tests. The yield stress is set to 13.0×10^9 dyne/cm^2 with strain hardening equal to 2% of the tensile modulus.

The failure criterion is based on reaching one of two conditions: (1) the accumulated plastic strains in both directions exceeds a specified limit, ε_{min}, set to 0.04 or (2) the accumulated plastic strain in a single direction exceeds a larger limit, ε_{max}, set to 1.20. When the fabric strain reaches ε_{min} in a single direction, the yield strength is dropped to 0.20 times the initial yield. This

response is used to simulate the residual strength in the fabric after held yarns break and the cross yarns redistribute the load. At failure, the loads in the fabric are reduced to zero over a strain value of 2%, and the element is eroded from the calculation.

Figure 28 shows the model stress-strain response under monotonically increasing uniaxial loading. As described above, the stress rises elastically to the yield stress of 13.0×10^9 dyne/cm^2, then increases with 2% hardening. When the plastic strain reaches ε_{min}, the load drops to 20% of the current stress, then hardening continues to a strain of 1.2, at which time failure occurs.

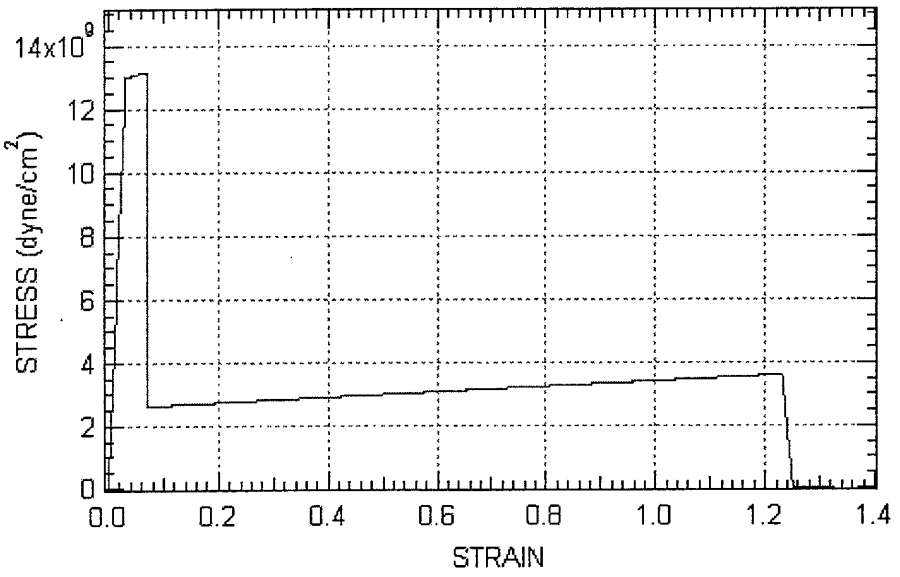

FIGURE 28. MODEL STRESS-STRAIN UNDER UNIAXIAL LOADING

For multiple plies, the fabric thickness is specified as the single-ply thickness and the values for modulus, yield strength, and density are multiplied by the number of layers. This strategy is used instead of multiplying the fabric thickness times the number of layers, to avoid unrealistically high bending strength. This model assumes that, for a multiple-ply target, the fabric yarns are all aligned in the same directions (e.g., 0 and 90 degrees).

Values for other moduli such as shear modulus, compression modulus, or crimp modulus should be small compared with the modulus in tension, but if these moduli are chosen as zero, the simulation typically crashes due to numerical problems. Thus, the values for these moduli are set to 2 % of the tensile modulus.

Fabric slack is also included in the model. The amount of slack is input as a strain value, ε_{sl}, as shown if figure 29. The effect of slack is to allow an initial strain to occur in the fabric without significant stress developing. Figure 29 shows the model stress-strain response under uniaxial loading, including slack and unloading.

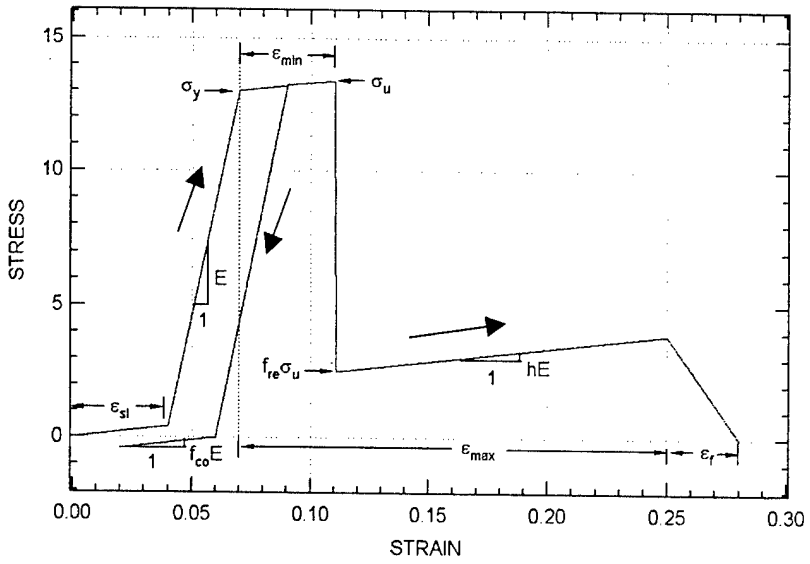

FIGURE 29. MODEL STRESS-STRAIN UNDER UNIAXIAL LOADING, INCLUDING SLACK AND UNLOADING

The fragment velocity at which the fabric is penetrated depends on the size of the elements around the impact location. If the elements are too large, the fabric appears too strong because the mesh is unable to capture the stress gradients around the fragment. If the model has too many small elements, the elements get tangled in the simulation and the simulation fails with numerical problems. As a result of these investigations, it is recommended that two to four elements be used across the smallest dimension of the fragment.

EXAMPLE SIMULATIONS.

PUSH TEST SIMULATIONS. Simulations were performed on two push tests, P-1 and P-15 [3]. P-1 was gripped on four edges and P-15 was gripped on two edges. Both specimens were single plies of 35x35 Zylon weave. Both tests used the standard 25-g fragment simulator as the penetrator. The fragment was aligned with the center of the specimen and oriented normal to the plane of the fabric (i.e., no pitch or yaw).

Although the experiments were performed quasi-statically, the simulations were performed dynamically with a fragment velocity of 10 m/s to allow for short calculation times. At this rate there is a small dynamic effect (due to inertia, the material model is not rate dependent) that shows up as a slight waviness of the force-displacement results.

Figure 30 shows the finite element mesh and configuration for push test P-1. The specimen has a cross-shaped geometry and is gripped on four edges. The specimen is 7.2 in. across with 1.1-in. cutouts at each of the four corners. The model has 3584, four-node thin-shell elements to represent the Zylon fabric. In the region of impact, an element size of 1.5 mm square gives four elements across the fragment edge.

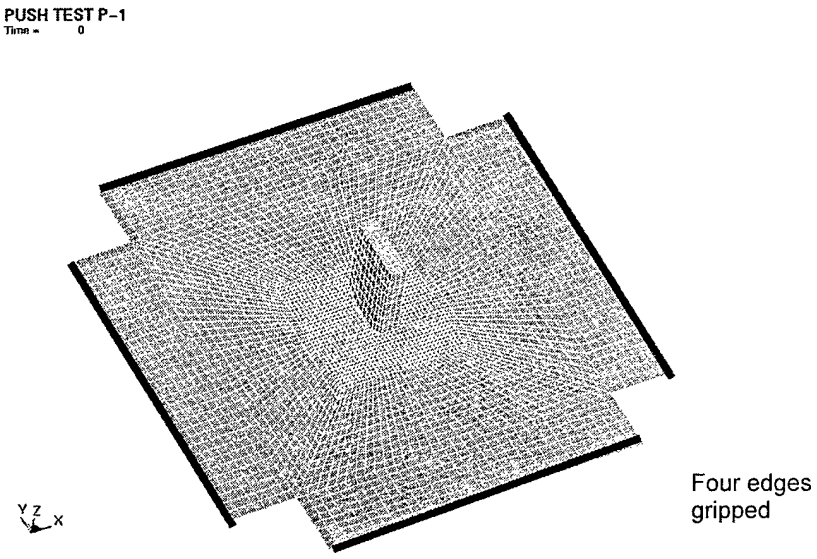

FIGURE 30. FINITE ELEMENT MESH FOR PUSH TEST P-1

Figure 31 shows the load-displacement curves for test P-1 for the experiment and the simulation. The load builds gradually with displacement as the fabric is stretched. In the experiment, the fabric fails catastrophically at a displacement of 0.77 in. In the simulation, the calculated load follows the measured load closely until the peak. Both the peak load and the peak displacement for the simulation are slightly greater than measured in the experiment. The peak load is about 13% higher (918 vs 814 lb) and the peak displacement is about 6.5% higher (0.82 vs 0.77 in.). The failure in the simulation does not happen as suddenly as in the experiment. This may be influenced by the dynamics of the response in the simulation.

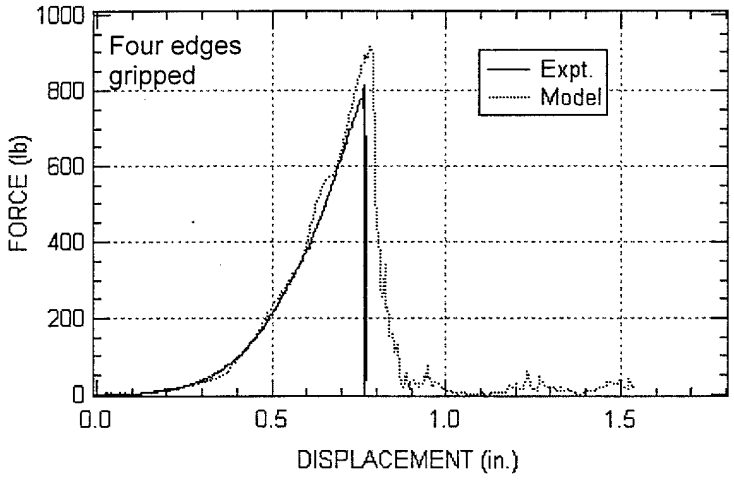

FIGURE 31. FORCE DISPLACEMENT FOR SIMULATION OF PUSH TEST P-1

Figure 32 shows the calculated damage to the fabric for push test P-1. The region of damage to the fabric is localized around the fragment.

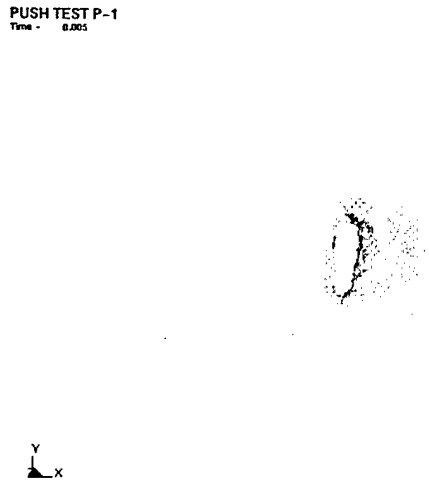

FIGURE 32. CALCULATED DAMAGE FOR PUSH TEST P-1

Figure 33 shows the configuration for push test P-17. The specimen dimensions are 7.2 in. by 5 in. The specimen is gripped along the two shorter edges and is oriented at 0 degrees relative to the gripped edges.

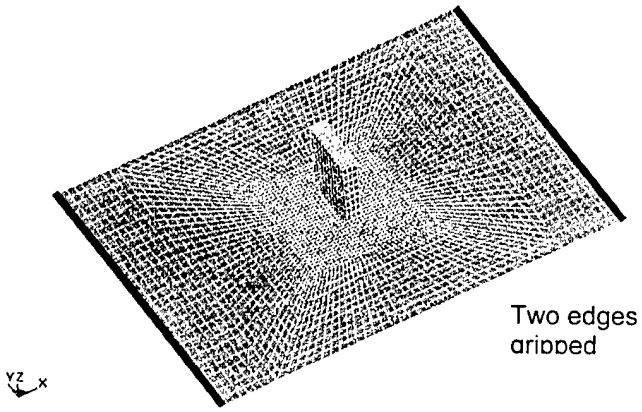

FIGURE 33. FINITE ELEMENT MESH FOR PUSH TEST P-17

Figure 34 shows the calculated and measured load-displacement curves for push test P-17. In both curves, the load increases monotonically to a peak. The calculated curve follows the measured curve closely during loading, but the calculated peak load and displacement are higher than the measured values. The calculated peak force of 671 lb is about 22% higher than the measured value of 550 lb, and the calculated displacement at peak load of 0.83 in. is about 4% greater than the measured value of 0.80 in. In the experiment, the load drops to about 300 lb after the peak and remains relatively constant out to a displacement of about 1.4 in. From 1.4 to 1.6 in., the measured load drops linearly to zero. In the simulation, the load drops to about 150 lb, then recovers and remains between 200 and 300 lb to a displacement of about 1.1 in., then drops to zero at about 1.2 in.

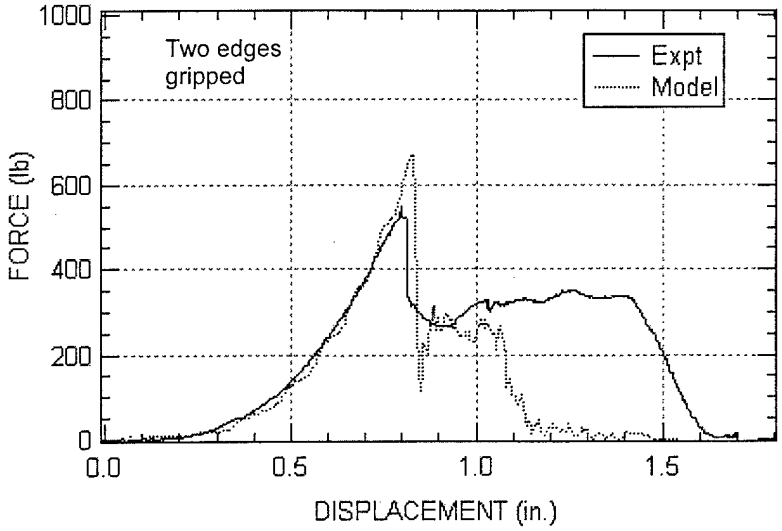

FIGURE 34. FORCE DISPLACEMENT FOR SIMULATION OF PUSH TEST P-17

Figure 35 shows the calculated damage to the penetrated fabric for push test P-17. As with the simulation for push test P-1, the damage is localized around the region of impact. In the experiment, however, damage was also observed in other locations. In addition to the damage around the impact site, yarn failure was observed near the grips and yarn pullout was observed along the ungripped edges.

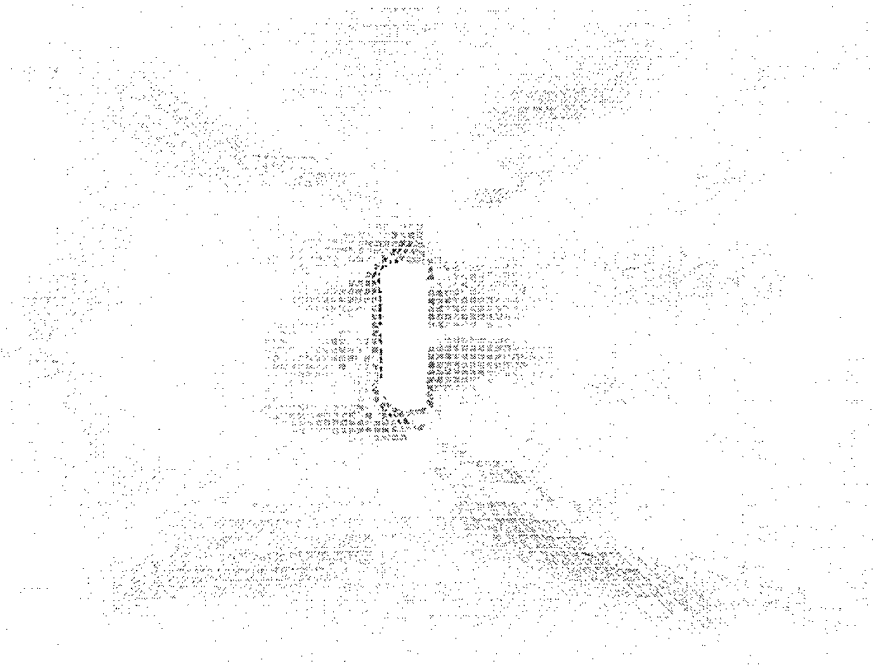

FIGURE 35. CALCULATED DAMAGE FOR PUSH TEST P-17

LABORATORY GAS GUN TESTS. Simulations were performed of gas gun tests 25 and 47 [3]. Both tests had a single ply of 35x35 Zylon. Test 25 had four edges gripped and test 47 had two edges gripped. In both tests, the fragment was the standard 25-g fragment simulator. In these calculations, the finite element mesh for the fabrics was the same as for the push tests, but the orientation of the fragment was modified to match that measured in the experiment.

Figure 36 shows the configuration for test 47. The fragment had an initial orientation of -6° roll and +1° pitch. In test 47, two edges were gripped. In figure 36, the gripped edges are the top and bottom edges. The response of the fabric is shown in figure 36(b) through 36(e), with the fragment moving right to left. In figure 36(a) through 36(c), the view is from the impacted side of the fabric. In figure 36(d) and 36(e), the view is from the back and the fragment is seen breaking through the fabric. As seen in figure 36(d) and 36(e), the fabric rips parallel to the gripped edges and drapes over the fragment, providing resistance as the fragment penetrates.

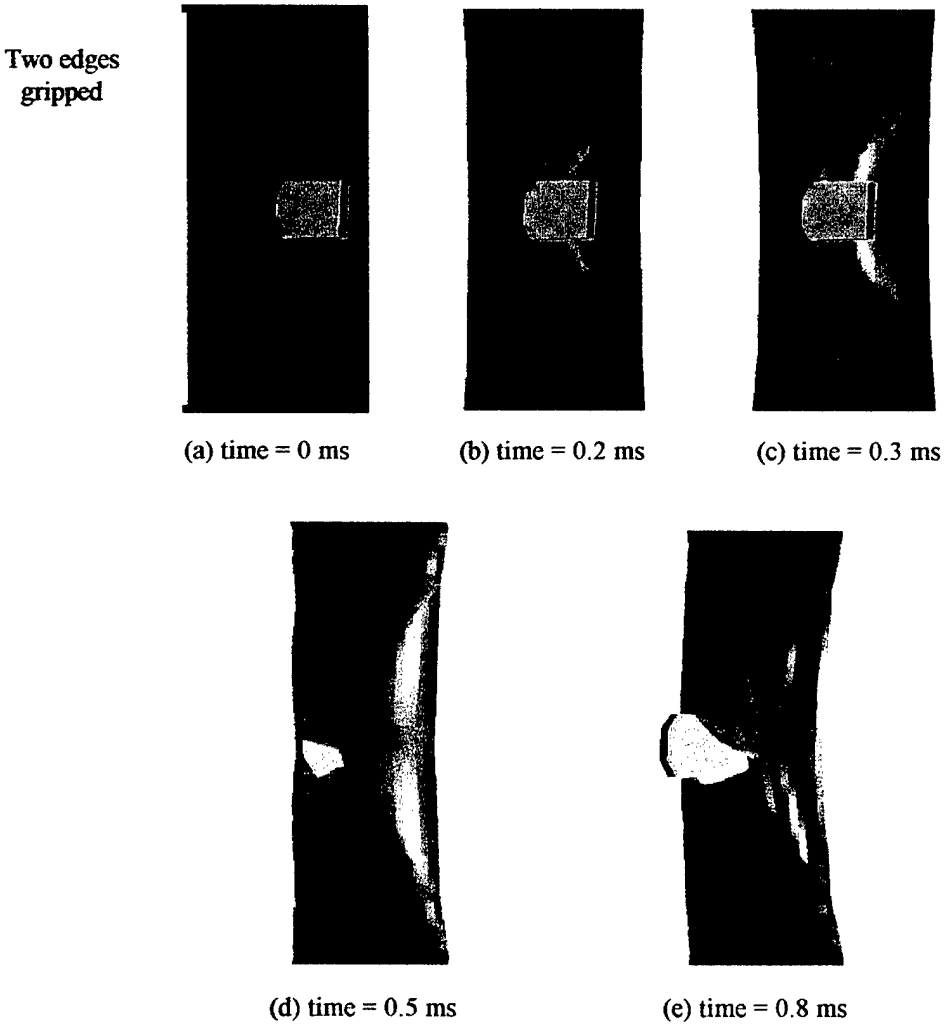

FIGURE 36. SIMULATION OF GAS GUN TEST 47

Figure 37 shows the calculated velocity of the fragment as it penetrates the fabric. The initial velocity was 80 m/s. The fragment penetrates completely at about 0.7 ms. The calculated value for the residual velocity of the fragment was 52 m/s, 5.7% greater than the measured value of 49.2 m/s. In this simulation, the calculated energy absorbed by the fabric was about 92% of that measured.

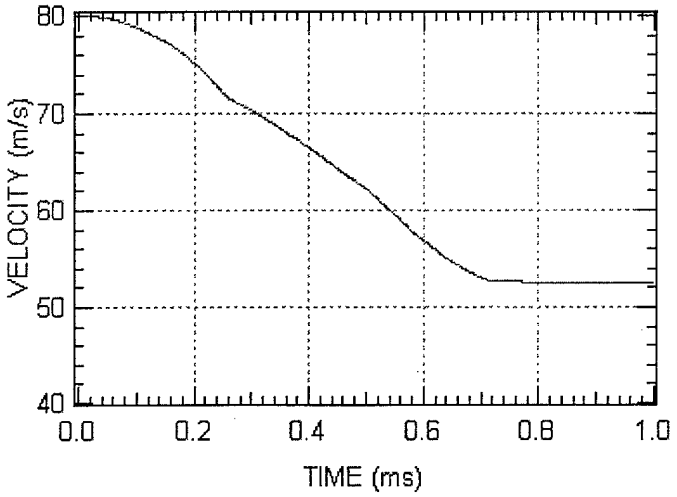

FIGURE 37. CALCULATED VELOCITY HISTORY OF FRAGMENT FOR GAS GUN TEST 47

Figure 38 shows the calculated force history on the fragment for gas gun test 47. The calculated peak load of 380 lb (test 47) is only about 56% of the calculated peak load of 671 lb (test P-17) for the push test result shown in figure 34. The calculated postpeak response in the gas gun test shows a force between 200 and 300 lb applied to the fragment as it penetrated the fabric.

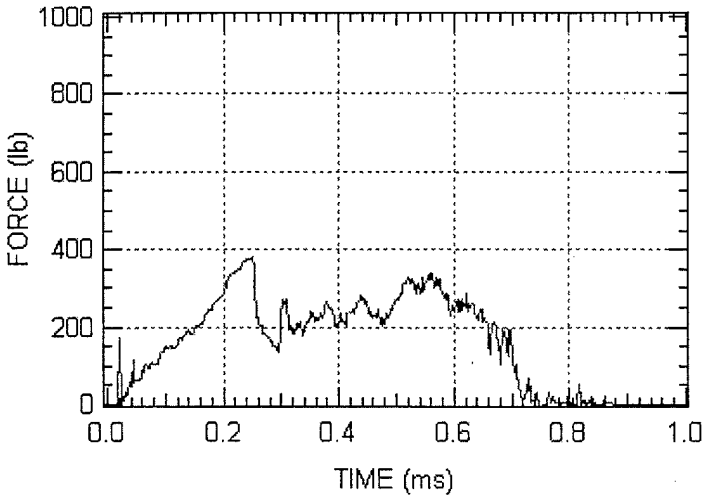

FIGURE 38. CALCULATED FORCE ON FRAGMENT FOR GAS GUN TEST 47

Figure 39(a) shows the configuration for test 25, which is a single ply of 35x35 Zylon with four edges gripped. The fragment had an initial orientation of -18° roll and 25° pitch. In the figure, the fragment is moving right to left. In figure 39(a) and 39(b), the view is from the impacted side of the fabric. In figures 39(c) though 39(f), the view is from the back, and the fragment is seen breaking through the fabric. As seen in figures 39(c) through 39(e), the fabric provides considerable interference as the fragment penetrates.

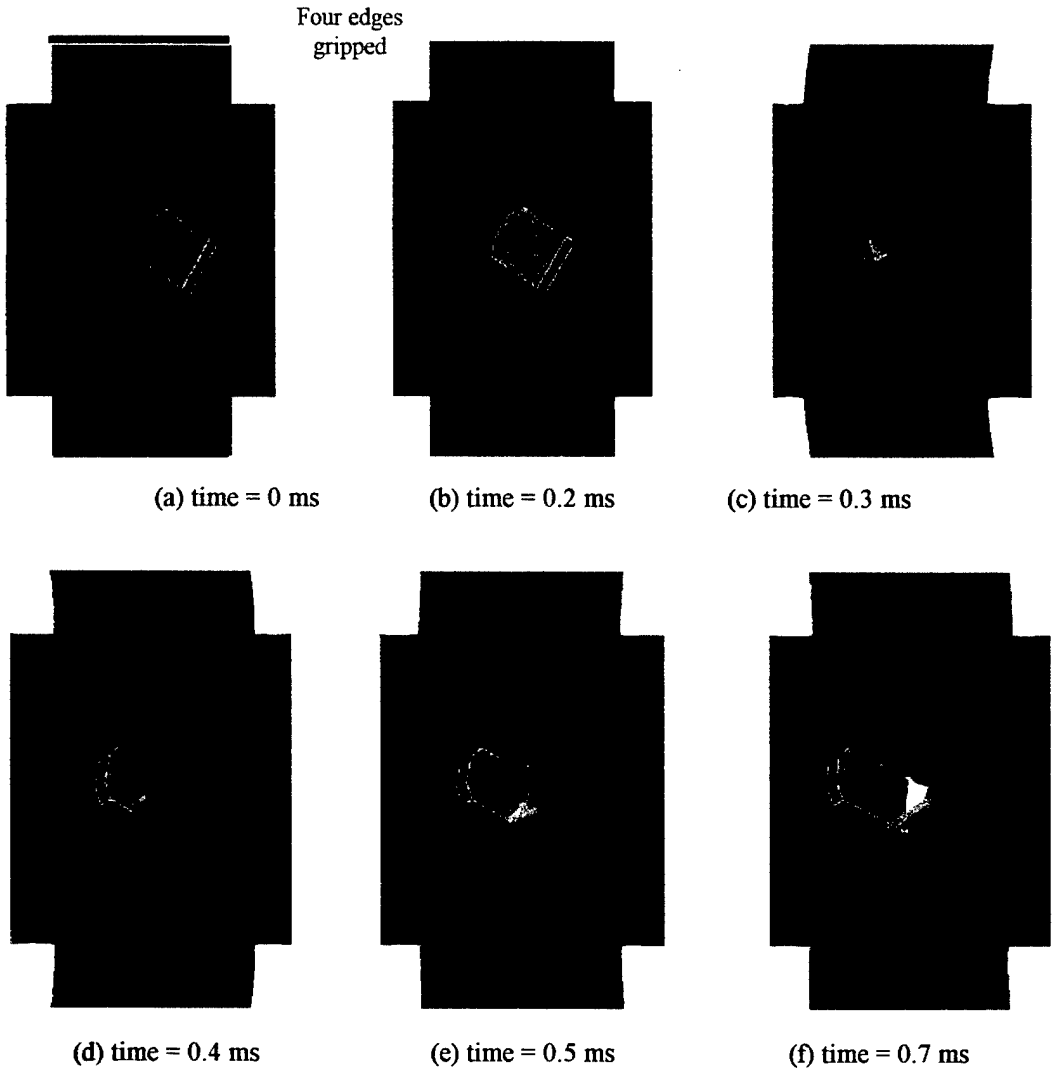

FIGURE 39. SIMULATION OF GAS GUN TEST 25

Figure 40 shows the calculated fragment velocity history for gas gun test 25. The initial velocity was 77.5 m/s. The calculated value for the residual velocity of the fragment was 43.6 m/s and the measured value was 59 m/s. The fabric model was significantly stronger in this simulation than in the experiment, and the calculated energy absorbed by the fabric was about 62% greater than that measured. This result is consistent with the push test results for the case with four sides gripped; the model overpredicts the resistance of the fabric.

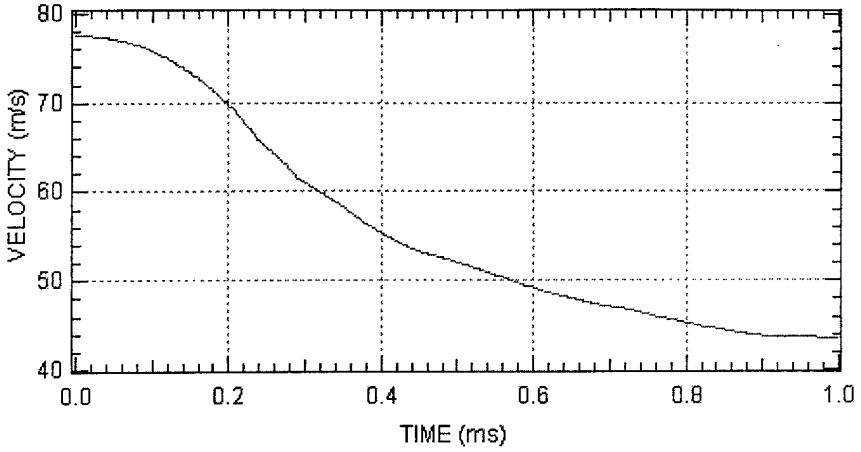

FIGURE 40. CALCULATED VELOCITY HISTORY OF FRAGMENT FOR GAS GUN TEST 25

Figure 41 shows the calculated force history on the fragment for gas gun test 25. In the simulation, the fabric exerts force on the fragment throughout the entire penetration process, probably because of the large amount of pitch and yaw in the fragment. The calculated peak load of 615 lb (test 25) is only about 2/3 of the peak load of 915 lb (test P-17) for the push test results shown in figure 31. However, the response to the push test showed a very abrupt drop in load after the peak, whereas the calculated force in the gas gun test drops slowly.

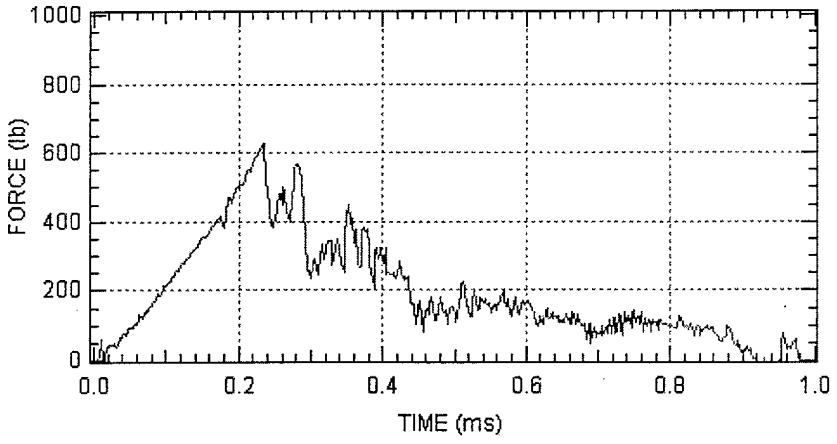

FIGURE 41. CALCULATED FORCE HISTORY OF FRAGMENT FOR GAS GUN TEST 25

LARGE-SCALE IMPACT TEST. A model simulation was performed on the large-scale impact test 119 described in the test results section. This test was performed using the 6-in.-bore gas gun facility at CHES. The configuration for the simulation is shown in figure 42. The barrier has overall dimensions of 34 x 24.6 in. and is attached at four 1-in.-diameter pegs positioned 21.25 in. apart in the vertical direction and 13 in. apart in the horizontal direction. The 189-g fragment impacts the center of the barrier with an initial velocity of 132 m/s and a roll angle of 29°. The barrier contains two layers of Zylon 35x35.

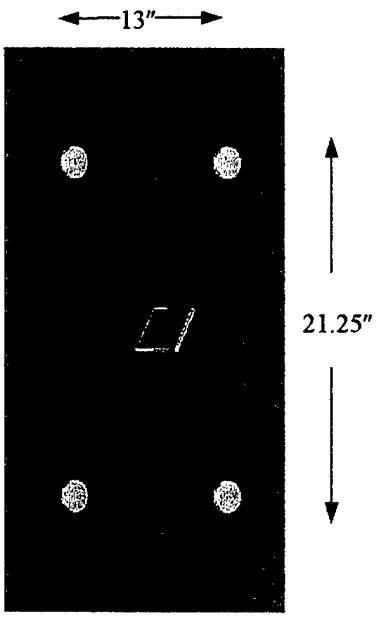

FIGURE 42. CONFIGURATION FOR SIMULATION OF LARGE-SCALE IMPACT TEST 119

The mesh for the simulation contained 7948 shell elements for the barrier and 6304 solid elements for the fragment and the attachments. Because the fragment is sharp, small elements were needed in the area of impact. An element size of 0.6 mm was chosen to give two elements across the fragment edge, as shown in figure 43.

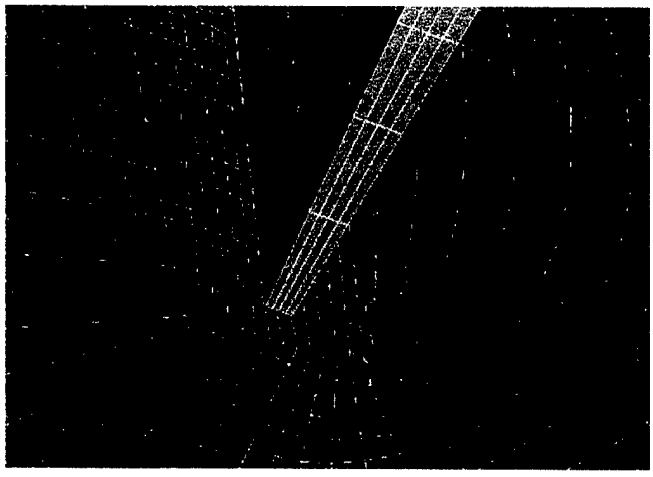

FIGURE 43. FINITE ELEMENT MESH IN FRAGMENT REGION FOR LARGE-SCALE IMPACT TEST 119

The calculated response of the barrier for large-scale impact test 119 is shown in figure 44.

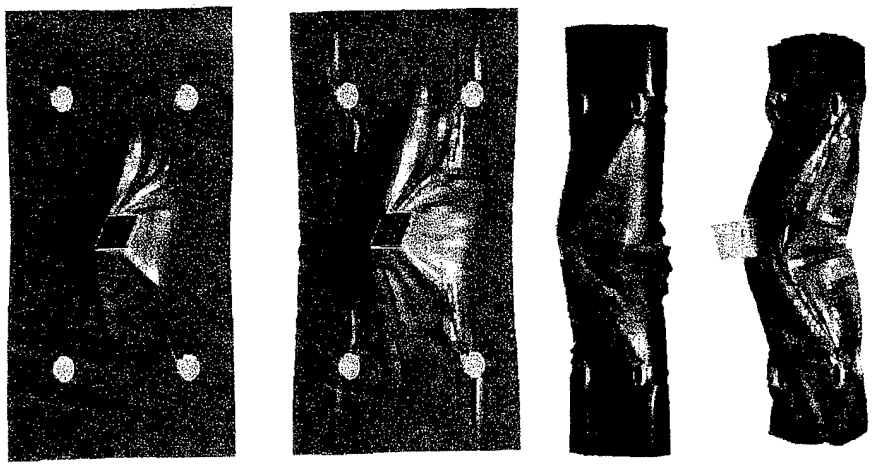

(a) 0.5 ms (b) 0.8 ms (c) 1.2 ms (d) 2.4 ms

FIGURE 44. CALCULATED RESPONSE OF LARGE-SCALE IMPACT TEST 119

The calculated velocity history of the fragment for large-scale impact test 119 is shown in figure 45. The calculated residual velocity of the fragment was 68.2 m/s, which is very close to the measured velocity of 66.4 m/s based on the average velocity of the four corners (calculated from the digitized position records). The calculated velocity appears to drop more suddenly than observed, indicating that perhaps the fabric is more compliant than the model. This could be due to slack in the fabric, which was set to zero for this simulation.

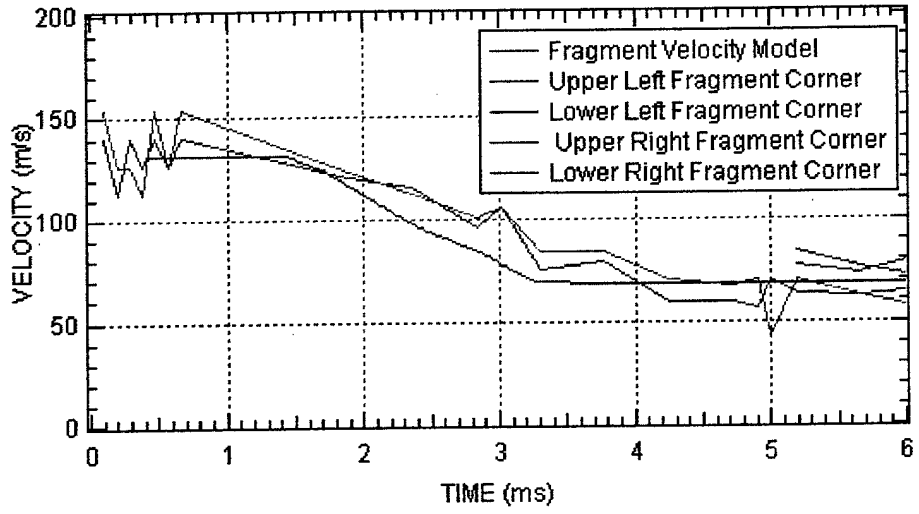

FIGURE 45. CALCULATED VELOCITY HISTORY FOR LARGE-SCALE IMPACT TEST 119

The calculated damage to the fabric in large-scale impact test 119 is shown in figure 46. The fragment penetrated the barrier very cleanly; the hole is only slightly larger than the fragment.

Some ripping occurred at the attachments. The extent of the ripping in the simulation varied from about 0.5 to 1.0 in. at the attachment points. In the experiment, ripping of 0.5-2 in. occurred at the attachments.

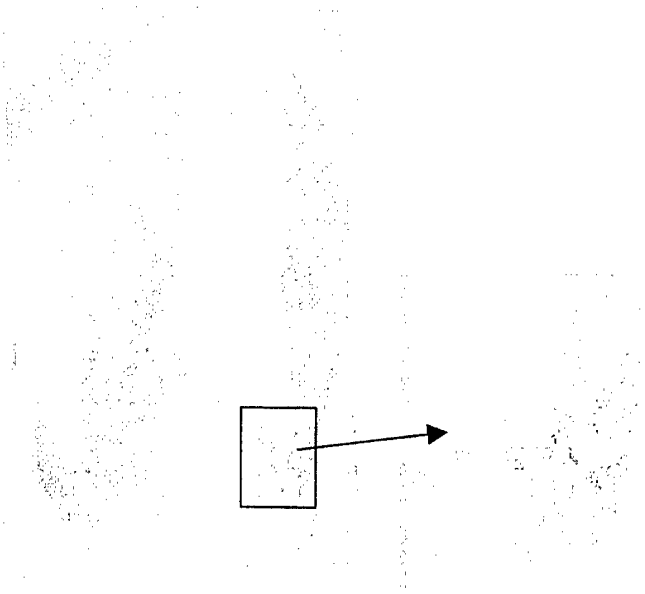

FIGURE 46. CALCULATED DAMAGE TO FABRIC FOR LARGE-SCALE IMPACT TEST 119

DISCUSSION OF COMPUTATIONAL DESIGN MODEL.

The design model has been used to simulate a series of tests on 35x35 Zylon. The result of these simulations is promising. With a single set of parameters, the model does a reasonable job on the following simulations:

- Quasi-static push tests. The simulations matched load-displacement curves up to failure for a single layer of Zylon fabric gripped on two edges and on four edges. The model clearly showed the difference in fabric stiffness for those two cases. The model correctly simulated the different modes of failure. For tests gripped on four edges, the failure is sudden; the load drops quickly after the first failure occurs. For tests gripped on two sides, the mechanism is quite different; significant load is carried after the initial damage to the fabric.

- Laboratory-scale gas gun tests. The model was used to simulate two laboratory gas gun tests. For a single layer of fabric gripped on two edges impacted by a 80 m/s fragment, the calculated residual velocity of 52 m/s was about 6% greater than the measured value of 49.2 m/s. The calculated energy absorbed by the fabric was about 7% less than that measured. For a single layer gripped on four edges impacted by a fragment at 77.5 m/s, the calculated residual velocity of 43.6 m/s was 26% less than the measured value of 59 m/s, and the calculated absorbed energy was about 60% greater than that measured.

- Large-scale impact tests. The model was used to simulate two layers of fabric attached at four corners and impacted by a sharp fragment at a velocity of 132 m/s. The model simulated the local tearing of the fabric around the fragment and also the ripping of the fabric that occurs at the attachments. The calculated residual velocity of 68.2 was within 3% of the measured value of 66.4 m/s, and the calculated energy absorbed was about 2% less than the measured value.

LIMITATIONS.

As formulated, the design model does have limitations, including the following:

1. Using continuum elements to model plain fabric produces a tendency of the fabric model to rip because of direct connectivity between adjacent elements. Real yarns do not transfer load directly to adjacent yarns because the physical connection is through yarn overlap.

2. For the cases with four edges gripped, the model overpredicts fabric resistance. In the experiments, the failure is very abrupt; in the simulations, the fabric has residual strength after the initial damage occurs.

3. Failure of the fabric is strongly influenced by element size. If the elements are too large, the fabric is too strong; if the elements are too small, the fabric gets tangled. For sharp fragments, simulations can take an extensive amount of computer time because small elements are needed to capture the stress gradients.

4. The failure mechanisms are not correct for static tests gripped on two edges; mechanisms observed in the experiments [3], including remote failure and yarn pullout, are not simulated in the model.

5. It appears the model needs to be more compliant in the large-scale tests, possibly because of difficulties in modeling the method of attachment (pegs through holes), slack in the fabric, or too much bending resistance of the shell model.

6. The model has been used for tests using only one or two layers of fabric; more tests and model development will be necessary to simulate barriers with several layers of fabric.

7. Input parameters have only been developed for Zylon AS 35x35 with 500 denier yarns. Input parameters for different weaves or different materials need to be developed by the user.

8. The effects of yarn crimp have not been properly modeled. In the current model, a slack strain is input, and the amount of slack is assumed to be the same in both directions, and does not depend on the loading history. In real fabrics, the amount of crimping in the yarns is different in the warp and fill directions, and the effects of crimp change under different loading conditions.

FUTURE PLANS

AIRWORTHINESS ASSURANCE CENTER OF EXCELLENCE (AACE) GRANTS.

Future work should focus on enhancing this model and transitioning the technology to industry. SRI will contribute to efforts in two FAA AACE Grants that were established in 2001.

- The grant with Arizona State University (ASU) includes Honeywell Inc. and NASA Glenn. The objective is to model and design high-strength fabric barrier systems for containing turbine engine fragments within the nacelle.

- A second grant with the University of California at Berkeley (UCB) includes Boeing Corp. The objective of this work is to model and design barriers for uncontained fragments for specific fuselage applications.

REFERENCES

1. Aircraft Catastrophic Failure Prevention Research Program Plan, January 1994, U.S. Department of Transportation, Federal Aviation Administration, Technical Center, Atlantic City International Airport, New Jersey, 1994.

2. Shockey, D.A., Giovanola, J.H., Simons, J.W., Erlich, D.C., Klopp, R.W., and Skaggs, S.R, "Advanced Armor Technology: Application Potential for Engine Fragment Barriers for Commercial Aircraft," DOT/FAA/AR-97/53, Federal Aviation Administration William J. Hughes Technical Center, Atlantic City International Airport, New Jersey, July 1997.

3. Shockey, D.A., Erlich, D.C., and Simons, J.W., "Improved Barriers to Engine Fragments: Interim Report III," DOT/FAA/AR-99/8,III, Federal Aviation Administration, William J. Hughes Technical Center, Atlantic City International Airport, New Jersey, May 2001.

4. Erlich, D.C., Shockey, D.A., and Simons, J.W., "Full-Scale Tests of Lightweight Fragment Barriers on Commercial Aircraft," DOT/FAA/AR-99/71, Federal Aviation Administration, William J. Hughes Technical Center, Atlantic City International Airport, New Jersey, November 1999.

5. Shockey, D.A., Erlich, D.C., and Simons, J.W., "Improved Barriers to Engine Fragments, Interim Report IV," DOT/FAA/AR-99/8,IV, Federal Aviation Administration, William J. Hughes Technical Center, Atlantic City International Airport, New Jersey, June 2002.

APPENDIX A—USER'S MANUAL FOR BALLISTIC FABRIC MODEL

A user's manual for the ballistic fabric model is given below. The format of the manual is consistent with the LS-DYNA3D User's Manual. Table A-1 gives values for material constants for a single ply of Zylon 35x35. These values were determined from quasi-static push tests and verified by dynamic gas gun tests as described in this report. The model has also been verified for two plies. For two plies multiply the modulus, yield stress and density by two, all other parameter values remain the same.

TABLE A-1. MATERIAL CONSTANTS FOR A SINGLE-PLY 35x35 ZYLON FABRIC

Name	Symbol	Value (cgs)
Density	ρ	0.832 g/cc
Tensile Modulus	E	4.2×10^{11} dyne/cm^2
Bidirectional failure strain	ε_{min}	0.04
Unidirectional failure strain	ε_{max}	1.20
Yield stress	σ_y	13.0×10^9 dyne/cm^2
Slack strain	ε_{sl}	0.0 (depends on attachments)
Shell thickness	t	0.019 cm

Columns	Quantity		Format
1-10	Card 3 Tensile modulus, E		E10.0
11-20	Bidirectional failure strain, ε_{min}		E10.0
21-30	Unidirectional failure strain, ε_{max}		E10.0
31-40	Yield stress, σ_y		E10.0
41-50	Slack strain, ε_{sl}		E10.0
1-10	Card 4 Compression factor, f_{co}	(default 0.02)	E10.0
11-20	Shear modulus, G	(default 0.02*E)	E10.0
21-30	Hardening factor, h	(default = 0.02)	E10.0
31-40	Residual strength factor, f_{co}	(default 0.20)	E10.0
41-50	Failure strain interval, ε_f	(default 0.10)	E10.0
61-70	Max. failure increment, d_{max}	(default 0.01)	E10.0

The ballistic fabric model is orthotropic with stress-strain response as shown in figure A-1 for each of the two yarn (local x and y) directions. The stress-strain responses in the two directions are uncoupled, but the failure response is coupled.

$$\sigma_{xx} = f(\varepsilon_{xx})$$
$$\sigma_{yy} = f(\varepsilon_{yy})$$
$$\sigma_{zz} = 0$$
$$\tau_{xy} = G\,\varepsilon_{xy}$$
$$\tau_{yz} = G\,\varepsilon_{yz}$$
$$\tau_{zx} = G\,\varepsilon_{zx}$$

As shown in figure A-1, the uniaxial response has the following features:

- Elastic response with modulus E up to yield stress, σ_y
- Linear hardening with modulus = hE
- Elastic unloading with reduced compression modulus = f_{co} E
- Slack before straightening, slack modulus = compression modulus
- Default shear modulus is small = 0.02*E
- Failure:

  If plastic strain reaches ε_{min} in one direction, the strength drops to a fraction of the stress at ε_{min}

  If plastic strain in both directions reaches ε_{min}, the element is failed

  If plastic strain in a single direction reaches ε_{max} the element is failed

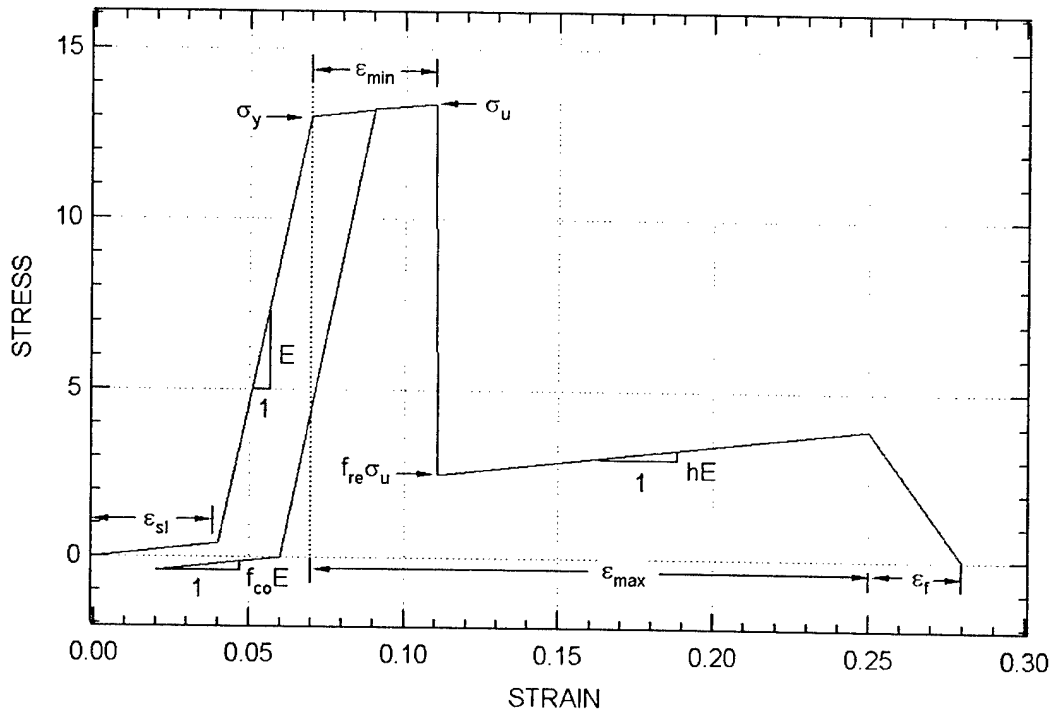

FIGURE A-1. UNIAXIAL STRESS-STRAIN CURVE FOR BALLISTIC FABRIC MODEL